Journal of *Marine Science and Engineering*

MDPI

Article

CFD Study on Hydrodynamic Performances of a Planing Hull

Florin Pacuraru, Andreea Mandru and Adham Bekhit *

Department of Naval Architecture, "Dunarea de Jos" University of Galati, Galati 800008, Romania
* Correspondence: adham.bekhit@ugal.ro

Abstract: The scope of the present study is to investigate the effects of various geometrical hull features, such as tunnels, spray rails and whiskers on the hydrodynamic performance of a high-speed planing hull. The criteria being tested to emphasize the boat performance are the total drag, sinkage and trim angle. In addition, the decomposition of the resistance into viscous and wave-making resistance are taken into consideration. The study starts with a validation test against experimental data in order to accentuate the capability of the Computational Fluid Dynamics CFD simulation to accurately predict the total drag and trim angle of the initial form. This is later followed by a verification study based on the Richardson Extrapolation method with a grid- and time-step-convergence test in order to predict the numerical errors during the simulation. After establishing the simulation parameters regarding the proper grid size and time step, the comparative study takes place for five hull shapes and two whisker configurations while the boat is sailing at eight different speeds. The assessment of the hydrodynamic flow parameters is evaluated compared to the initial form in order to investigate the influence of the geometry change on the hydrodynamic performances of the boat. Validation of the numerical results showed the reliability of the CFD simulation to accurately predict the drag and trim angle of the boat, while the comparative study revealed that the total drag can be reduced by up to 9%, especially at higher speeds.

Keywords: high-speed boat; planing hull; RANS; VOF; spray rails

Citation: Pacuraru, F.; Mandru, A.; Bekhit, A. CFD Study on Hydrodynamic Performances of a Planing Hull. *J. Mar. Sci. Eng.* **2022**, *10*, 1523. https://doi.org/10.3390/jmse10101523

Academic Editors: Simone Mancini and Momchil Terziev

Received: 30 September 2022
Accepted: 10 October 2022
Published: 18 October 2022

1. Introduction

A planing hull is a special marine vessel that depends, in its common operational condition, on the hydrodynamic pressure lift to maintain its equilibrium in the vertical direction. This concept differs from the displacement hulls that depend on the hydrostatic pressure distribution around the hull. Initially, and at low speeds, the planing vessels are performing as the displacement hulls; however, the common operation of the planing hull is distinguished by the transition from displacement to planing regime through a transitional stage that is called the preplaning regime, since the basic feature of the planing vessel is to perform in high-speed conditions. This principal feature made them propitious for military, racing, transport and search and rescue applications. On the other hand, it also makes their hydrodynamic performance a very challenging and complicated task due to the presence of multiple complex hydrodynamic phenomena, such as flow separation, ventilation, spray, wave breaking, etc. This topic has been a major concern for researchers in the marine hydrodynamic domain since the early 1930s. Reviewing the state of the art for the hydrodynamic performance of the planing hulls can categorize the possible methods used in this scope into three major groups: experimental, analytical and numerical techniques. In addition, one may observe that the sequence of applying these techniques does not differ much from the displacement hulls, in which the experimental approach initially took place. The analytical methods came after to assess the data of the performed experiments in order to generalize the hydrodynamic aspects of concern from the regression of the data gathered from the experiments, resulting in empirical formulas and methodical series. Finally, the numerical stage leads the domain after and alongside the computer

development, which helped in initially applying the potential-flow and later the viscous-flow modeling approaches that analyze the complex flow phenomena with less physical assumptions.

The initial stage, as previously introduced, started with experimental approach that dominated the analysis of the hydrodynamic characteristics of the planing vessels till the 1960s, when the experimental studies on hydrodynamic characteristics of constant dead-rise prismatic planing surfaces had been reported by Sottorf [1], Shoemaker [2] and Sambraus [3]. Later on, Savitsky made a significant contribution to the understanding and evaluation of planing hulls, clarifying further the hydrodynamics of planing surface phenomena [4–6]. He also developed a semi-empirical correlation for prediction of lift and drag forces that act on planing hulls [7]. Furthermore, over the past several decades, many extensive model tests were conducted to evaluate the hydrodynamic performance of the planing hulls, resulting in the well-known series such as series 62 [8], Series 65 [9,10] and, more recently, the work reported in [11–14] that correlated the effects of the hull-design variable changes on the performances of the hull. Furthermore, the experimental approach also established a fundamental reference database for the numerical simulation validation purposes which are still in use so far.

The analytical and empirical approach could be linked, as previously stated, with the experimental approach, benefitting from the database collected during the experiments to set the standards for the hull series and regression-based analysis. A comprehensive review of planing and preplaning hull-resistance prediction methods based on hull series, regressions and empirical approaches was reported by Almeter [8]. The link between the two approaches was highlighted by Yousefi et al. in their comprehensive review for planing-hull analysis techniques reported in [14], wherein they categorized both methods in a single approach, calling them analytical–experimental techniques.

With the development of computers, numerical technique took the lead and started to develop over the past six decades. Potential growth started with the 2D, followed by the 3D analysis approaches, in addition to applying various flow modeling methods, such as potential flow and later the viscous flow analysis. Numerical techniques can be used to determine the flow parameters and estimate the hydrodynamic behavior of planing vessels. Though it was conducted successfully in multiple applications, there are several aspects concerning the hydrodynamics of planing hulls that makes their investigation much more complicated than displacement hulls. This is due to the spray drag, wave-making drag, the two-phase nature of the flow and numerical ventilation [15]. These are the reasons why accurately capturing the dynamics of the planing hull is still a challenge for the numerical approach, as previously stated.

The earliest theoretical research on planing hydrodynamics was based on a 2D approach, wherein the method was basically analytical and very limited. This was later followed by a 3D approach, such as the work efforts reported by Tulin [15], Maruo [16] and Wang and Rispin [17]; nevertheless, their work was characterized by the restriction of aspect ratio or planing speed [18]. Later, in the attempt to overcome these restrictions, Doctors [19] developed a method based on the finite pressure elements to represent the wetted surface of the planing area; however, the obtained pressure distribution was significant oscillatory. The problem of pressure oscillation has been investigated by Cheng and Wellicome [18], developing a pressure strip method, as well as by Xie et al. [20], using vortex theory and the finite element approach. A strip theory for steady planing in calm water was introduced by Zhao et al. [21]. The important achievements were based on the potential flow relayed on the boundary element method (BEM). Ghassemi [22–25] refined a combined method based on a potential-based BEM for the induced pressure resistance, the boundary layer theory for the frictional resistance and empirical technique for the spray resistance.

Simulation of the flow around planing crafts is rather complex, as it supposes to capture various hydrodynamic phenomena that have different lengths and time scales, as plunging jet, turbulent boundary layer and wave braking [26]. Despite the advantage of the potential-flow methods that can be summarized in their simplicity, low cost and less simu-

lation efforts, they always suffer significant limitations since they ignore the viscous effect that dominates most of these phenomena. The growth of the computational power allows viscous methods based on Reynolds-averaged Navier–Stokes (RANS) to become used for high-speed craft hydrodynamics studies. The finite volume method (FVM) dominates the discretization category for the hydrodynamic performance of high-speed planing hulls with rare applications of the finite difference method and finite element method [14]. The FVM, unsteady RANS with the free surface captured based on the volume of fluid (VOF) has been found to be the most effective solution for the prediction of planing hydrodynamics performance, as reported in [27]. The discretization in space is usually conducted with single mesh supported with local refinements in the separation and free-surface zones to stand for significant grid deformation and, most commonly, the use of overset or morphing grids are also applicable in a wide range of planing hull simulations. The first attempts that used RANS-VOF for high-speed planing flow investigation were reported by Camponneto [28] and Azcueta [29], who used the capabilities of the Comet commercial RANS-VOF solver. To a similar extent, Mancini et al. [30] validated a numerical simulation of a model-size planing boat using two solvers, FINE^{TM}/MARINE and STAR-CCM, against the data of the Naples Systematic Series model. The study showed the capability of CFD solvers in accurately capturing the hydrodynamic aspects of the planing hull. The study also included a verification test for predicting the numerical errors associated in the simulation. The verification task was also indicated by Manchini to be problematic [31], showing that there are possibilities to improve the reliability of numerical simulations of the planing vessels by reducing the errors. In addition, the verification and validation of numerical errors and uncertainties can contribute to enhance the modeling of the physics of planing crafts in order to increase their numerical simulation reliability. Wheeler et al. [32] conducted a numerical study to analyze the hydrodynamic performance of heavily loaded hard-chine hulls in calm water for concave- and convex-shaped hulls. The study concluded that the hulls with a concave bow had favorable hydrodynamic characteristics in term of drag resistance in both displacement and preplaning regimes for fully and nominal loading conditions. Some examples for investigations regarding the geometrical modification by introducing longitudinal rails besides the scale effect on the hydrodynamic performance of the planing hulls can be found in [33] and [34], respectively. The scope of studying the nonlinear and complex-flow phenomena developed in the planing hulls based on viscous-flow solvers, such as air cavity under a stepped planing hull, can be found in [35], while Wang et al., in [36] proposed a twin-side hull to overcome the porpoising instability of a planing hull, comparing the single-hull configuration with the formed trimaran concept. Further studies for the use of an FDM solver and the application of the DES approach in predicting the hydrodynamic performance of the planing vessels can be found in [37–39].

Concluding the aforementioned review and linking it to the present study while establishing the scope and motivation, the following ideas can be summarized: the planing hulls represent a special category of marine vehicles considering their operational aspects, which are mainly characterized by their high-speed performance. Multiple approaches and techniques have been used to study the hydrodynamic performance of the planing hull and the influence of modifying the geometrical design aspects on that hydrodynamic performance, out of which the experimental techniques remain as a reliable milestone method that has been recently used for validation purposes. At the same time, the RANS method started to take the lead in the numerical investigation of the planing hull hydrodynamic performance. Unlike the displacement ships that are supported by the hydrostatic forces acting on the hull, planing vessels are mainly sustained by the hydrodynamic forces. Plus, there are different geometrical features that planing hulls use to reduce drag and increase the lift of the boat over the water surface. This basically allows the planing vessel to sail faster compared to the displacement ship using the same propelling force [14]. This can have a beneficial outcome that contributes to the power optimization of the vessel. Heading from that concept and taking into consideration the fact that reducing the greenhouse and pollutant gases is one of the most important, yet challenging tasks in recent years. This is a

fact that obliged The European Commission to propose in its future vision, which is known as "European Green Deal", for the greenhouse gas emissions to adapt the EU climate, energy, transport and taxation policies in order to reduce the net greenhouse gas emissions by at least 55% by 2030 compared to 1990 and, consequently, to reach zero net greenhouse gas emissions and economic growth by the year 2050. Furthermore, in the new context of the fuel price increasing and the continuous challenge for switching to electric propulsion, each improvement of the hydrodynamic performance, even for planing boats, becomes absolutely necessary. The main reason behind the design optimization of motorboats lies on the need to maximize fuel efficiency, with advantageous outcomes in terms of cost-saving and environmental protection. In the scope of this principle, the current study takes place, which focuses on investigating the effects of various geometrical hull features in the planing hull design, such as tunnels, spray rails and whiskers, on the hydrodynamic performance of a high-speed planing hull. The geometry, position and configuration of these design elements are tested through the analysis of seven different categories that combine them in a systematic approach in order to emphasize and understand their influences on the hydrodynamic performance of the planing hull.

2. Geometries and Analysis Conditions

The study includes two main geometries; the first is used for a validation purpose wherein the EFD data are available [13,30], while the second is the main geometry wherein the comparative study takes place. The first geometry is depicted in Figure 1, showing a simple boat geometry with an overall length of L_{OA} = 2.611 m, a mean dead rise of 14° and a bottom spray rail. The complete characteristics for this geometry are listed in Table 1. The analysis conditions for this case correspond to a towing tank test performed and reported in [30], wherein the ship was towed at various speeds, starting with 2 m/s and ending with 7.5 m/s, with a step 0.5 m/s. For this study, the target is to estimate the total resistance and the trim of the boat during the sailing condition.

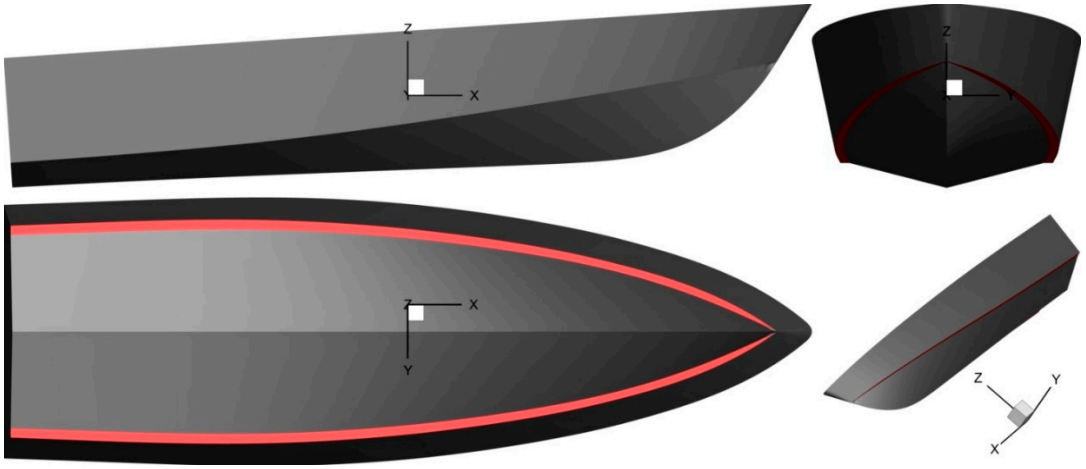

Figure 1. Validation case geometry showing profile, front and bottom views, respectively.

Table 1. Validation case dimensions and main characteristics.

Dimension	Unit	Value
Length overall	(m)	2.611
Draught	(m)	0.168
Beam at waterline	(m)	0.743
Longitudinal center of gravity (LCG)	(m)	0.944
Displacement	(kg)	106.7
Mean deadrise angle	(°)	14.00
Speeds	(m/s)	2.0–7.5

On the other hand, the second geometry, shown in Figure 2, depicts the most complex geometry in the comparative analysis, denoted with the abbreviation V7. The basic geometry forms a simple boat configuration with a tunnel. In addition, additional whiskers are added to study their influence on the boat performance. The main characteristics of the boat with its seven altered features are listed in Table 2, wherein every geometrical variation proposed is denoted with 'Vn' (i.e., V1 denotes the principal geometry, while the other variables include a modified tunnel geometry/dimensions or the addition of a whisker or two correspondingly).

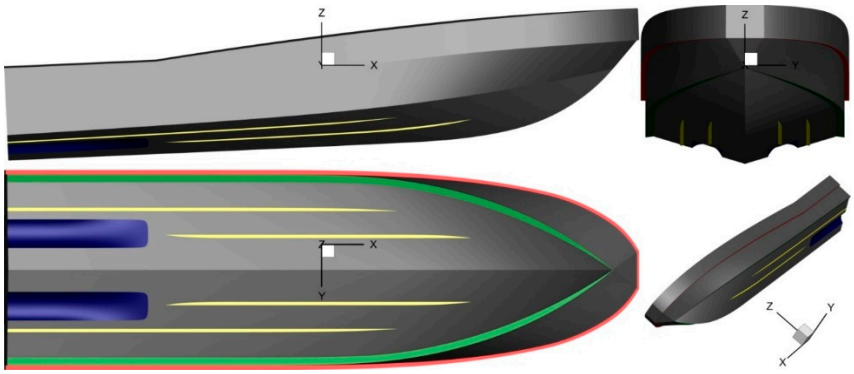

Figure 2. The boat geometry for V7 showing profile, front, bottom and isometric views, respectively.

Table 2. Test cases and hull characteristics.

Dimension	Unit	V1	V2	V3	V4	V5	V6	V7
Length overall	(m)	12.28	12.1	12.1	12.1	12.1	12.28	12.1
Waterline length	(m)	10.998	11.012	11.04	11.011	11.011	10.998	11.011
Draught	(m)	0.74	0.75	0.77	0.75	0.75	0.74	0.75
Beam	(m)	3.63	3.63	3.63	3.63	3.63	3.63	3.63
LCG	(m)	4.157	4.157	4.157	4.157	3.957	4.157	4.157
Displacement	(t)	14.288	14.288	14.288	14.288	14.288	14.288	14.288
Deadrise angle (X = 6.0 m)	(°)	19.7	21.0	22.0	21.5	21.5	19.7	21.5
Wetted surface	(m^2)	40.55	40.88	41.52	40.82	40.82	40.57	41.38
Spray rail width	(m)	0.11	0.11	0.19	0.15	0.15	0.11	0.15
Whiskers number	(–)	-	2.0	-	-	-	-	4.0
Tunnel length	(m)	2.18	2.18	2.675	2.675	2.675	2.675	2.675
Speeds (4 kn step)	(kn)	12-40	12-40	12-40	12-40	12-40	12-40	20-40
No. of computations	56	8	8	8	8	8	8	8

The simulation condition indicates the boat sailing in an open sea with a speed range from 12 knots to 40 knots, with a speed step of 4 knots in every simulation, resulting in 8 speeds/geometry and a total 56 simulation cases. The foremost target in this study is to compare the main hydrodynamic characteristics (such as: drag, lift, trim, air entrapment, etc.) of the boat as a result of the geometrical change.

3. Numerical Framework

3.1. Numerical Solver

The numerical solver used in this study is the ISIS-CFD flow solver of the FINE^{TM}/Marine software provided by NUMECA (now Cadence). The solver was developed by the EMN (Equipe Modélisation Numérique), i.e., numerical modeling and fluid dynamics team. It is based on the finite volume method to build the spatial discretization of the transport equations to solve the incompressible unsteady Reynolds-averaged Navier–Stokes equations (RANSE). The spatial discretization is face-based, while the temporal discretization is cell-centered, using a second-order three-level scheme. The velocity field is obtained from

the momentum-conservation equations and the pressure field is extracted from the mass-conservation constraint, or continuity equation, transformed into a pressure equation [40]. Velocity and pressure coupling are carried out using the semi-implicit method for pressure-linked equations (SIMPLE) algorithm. Convection and diffusion terms in the governing equations are discretized using a second-order upwind and a central-differencing scheme, respectively.

Closure to turbulence is achieved by introducing additional transport equations for modeled variables, which are solved in a similar form identical with that of the momentum equations and they can be discretized and solved using the same principles. The turbulence model used for the current study is the k-ω SST model [41].

The free-surface is modeled using a multiphase flow approach, based on the volume of fluid (VOF) free-surface capturing technique. Incompressible and nonmiscible flow phases are modeled through the use of conservation equations for each volume fraction of phase/fluid [42].

3.2. Governing Equations and Turbulence Modeling

The time averaged continuity and momentum equations for the incompressible flow with external forces can be written in tensor form, in the Cartesian coordinate system as

$$\frac{\partial(\rho\overline{u}_i)}{\partial x_i} = 0 \tag{1}$$

$$\frac{\partial(\rho\overline{u}_i)}{\partial t} + \frac{\partial}{\partial x_j}\left(\rho\overline{u}_i\overline{u}_j + \rho\overline{u_i'u_j'}\right) = -\frac{\partial\overline{p}}{\partial x_i} + \frac{\partial\overline{\tau}_{ij}}{\partial x_j} \tag{2}$$

where $\overline{u}_i$ is the relative averaged velocity vector of flow between the fluid and the control volume, $\overline{u_i'u_j'}$ is the Reynolds stresses, $\overline{p}$ is the mean pressure and $\overline{\tau}_{ij}$ is the mean viscous stress tensor components for Newtonian fluid under the incompressible flow assumption, and it can be expressed as

$$\overline{\tau}_{ij} = \mu\left(\frac{\partial\overline{u}_i}{\partial x_j} + \frac{\partial\overline{u}_j}{\partial x_i}\right) \tag{3}$$

3.3. Computational Domain and Boundary Conditions

The computational domain is constructed as a rectangular prism for which the dimensions in the (x-, y- and z-) directions are imposed as (7.5 L_{OA}, 2.0 L_{OA} and 2.0 L_{OA}), distributed as follows: the upstream inflow boundary is located at 1.5 L_{WL} from the forward perpendicular (FP); the outflow is located at 5.0 L_{OA} downstream from the aft perpendicular (AP); the side boundary are set at 2.0 L_{OA} from the centerline of the boat; top and bottom boundaries are chosen to be at 0.5 L_{OA} and 1.5 L_{OA}, above and underneath the undisturbed free-surface level, respectively. The undisturbed free-surface level is set at the ship design draft. Figure 3 depicts the computational domain and the boundary conditions of the exterior boundaries. Since the boat is sailing in the straight-ahead direction with no lateral forces and taking into consideration that only the vertical motions are included in this simulation, a symmetry approach is applied by introducing only half ship in the simulation to reduce the computational effort while maintaining the number of grid cells within a feasible level. The boundary conditions are set on the domain boundaries and the ship surfaces, as highlighted in Figure 3. A slip condition was set on the deck surface, assuming that it remains in air during the simulation, where the density of air compared to that in water can be neglected. The no-slip condition was set on the boat surfaces, while the wall is treated based on a wall function, with the y^+ computed automatically for the best fit based on the boat speed and initial grid during the insertion of the viscous layers. The typical range for the boat simulation is within $y^+ > 60$.

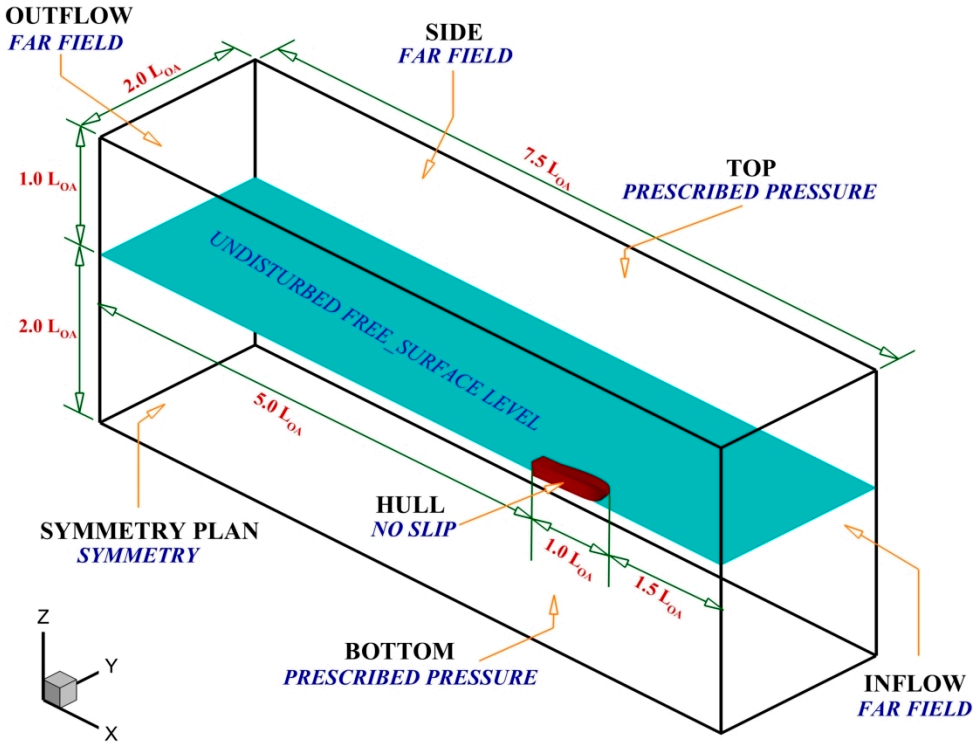

Figure 3. Computational domain and boundary conditions.

3.4. Discretization Grids

The discretization grids are generated using the HEXPRESS^{TM} grid generator included in the FINE^{TM}/Marine package, which generates nonconformal body-fitted full hexahedral unstructured meshes on complex arbitrary geometries. In addition, the advanced smoothing capability provides high-quality boundary layers insertion. In order to maintain the grid consistency between the various geometries included in this study, the main grid generation parameters, such as domain size, the initial number of cells, number of refinement layers on surfaces, curves and free-surface, global and local refinement diffusions and, finally, the number of viscous layers inserted in the boundary layers are maintained the same. The grid was initially generated for the grid-convergence study on the simple geometry boat provided with the experimental data in [13,31] to predict the suitable grid size and the optimal number of cells for the current comparative study. An isotropic refinement box was generated in the vicinity of the hull to capture more details of the flow and maintain the grid integrity in the stern zone, since the separation of the flow in that zone is considerably significant. In addition, a proper refinement of the free-surface is considered through a Kelvin-pattern refinement configuration sector that is added on the free surface and extended for only one times the boat length astern the hull to capture the free surface, accordingly, and to avoid any possible twisted or tangled cells during the simulation. However, the number of grid cells per wavelength in this region is kept within a relatively coarse level, because the free-surface configuration is not of concern in this comparison, though it remains important. To provide a spot on the grid configuration, the mesh for the most complex geometry (V7) is brought to attention in Figure 4. The other geometries are similar with respect to their geometrical conditions; the only difference exists in the presence or absence of the whiskers or the tunnel dimension, as previously explained in the geometry section. The principal grid density and configurations remain unchanged, regardless of the geometry, as previously mentioned, to maintain the consistency and the reliability of this comparison. The total number of grid cells for the different simulation cases are summarized in Table 3.

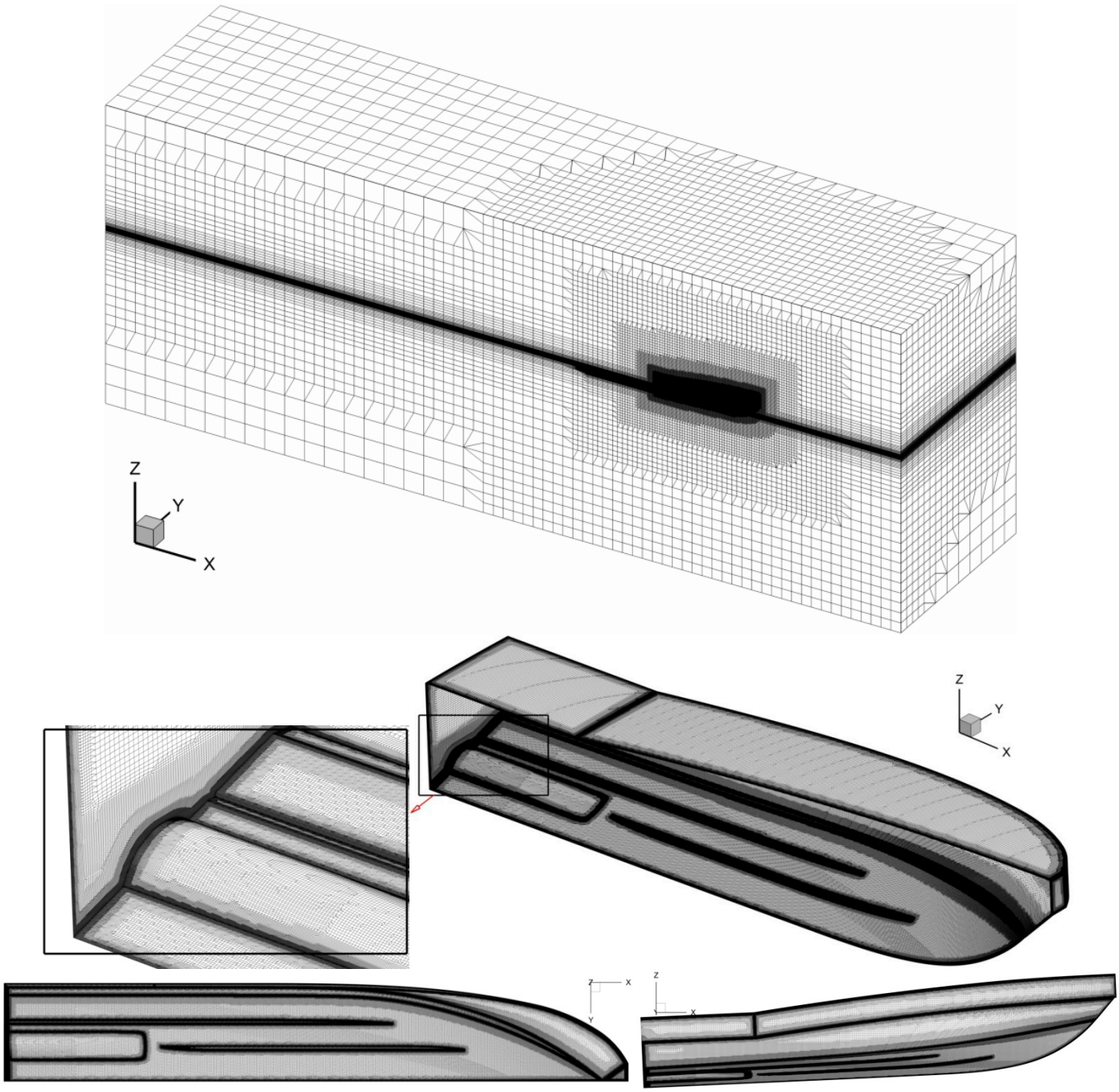

Figure 4. The finest discretization grid for the complex geometry V7, showing, respectively, a 3D domain grid, a 3D hull grid and bottom and side views.

Table 3. Number of grid cells for simulation cases.

Validation Study	**M3** 2.654	**M2** 4.316	**M1** 7.139			**$r_G \cong 1.65$**	
Grid Convergence Study Number of Grid Cells *10^6	**M4** 10.826	**M3** 15.230	**M2** 23.403	**M1** 34.027		**$r_G \cong 1.45$**	
Comparative study Number of Grid Cells *10^6	**V1** 10.326	**V2** 11.113	**V3** 9.922	**V4** 9.963	**V5** 10.561	**V6** 10.211	**V7** 15.230

3.5. Simulation Strategy and Computational Resources

The simulation is performed in a fully unsteady mode. All simulations are conducted as the boat sails in calm water conditions at the corresponding speed range V = 12:40 kn, with a step ΔV = 4 kn. An overlapping approach is used to accelerate the simulation, wherein the ship starts from the static position, i.e., ship speed is V = 0 kn, until it reaches the initial speed V = 12 kn. The acceleration period in this case is chosen based on the ship speed and boat length is T_{acc} = 2.0 L_{OA}/V. Afterwards, the overlapping takes place to reduce the acceleration period by half, starting with the initial speed in every speed step. The time step in each simulation is chosen with respect to the ITTC-recommended procedures for resistance simulation [43], as ΔT = 0.005 L_{OA}/V; yet, in this study, we use the time step as ΔT=0.001 L_{OA}/V, which is five times less, to ensure less time step errors. In addition, the total number of iterations is set to 10 in order to maintain the residuals in a confined level. Only two degrees of freedom are considered in this simulation, including the vertical motions sinkage and trim. The validation and verification studies are performed initially on the simplified geometry to set the base for the comparative study in order to establish the best practice for selecting an optimal time step and grid size. All the numerical simulations are performed on a high-performance computing (HPC) machine with 120 cores available, at a processing speed of 2.5 up to 3.3 GHz. The total computational time for first set of simulations regarding the verification and validation study was within 8–31 physical hours, while for the comparative simulations, the total physical computation time was within 8–10 h for simple geometries and 12–14 h for complex geometries with whiskers. The reason for the physical time variation is definitely related to the grid resolution and the time step used in the simulation.

4. Results

4.1. Validation and Verification

The validation of the numerical results was conducted based on the direct comparison with the experimental data provided in [13,31]. The verification study was performed at two levels: the first was dedicated for the model scale case based on a grid- and time-step-convergence study in order to choose the optimal numerical analysis parameters, referring to the mesh size and the time step. On the other hand, the second verification study was made at the full-scale level, since it is possible that the considerable difference in boat dimensions may encounter or result in additional numerical errors.

4.1.1. Validation

Initially, for the validation results, the coarsest grid M3 is fully analyzed at the total speed range, while for the finer grids, only three speeds are analyzed to grasp an insight through the solution change based on changing the mesh configuration. Figure 5 depicts the numerical simulation results compared to the experimental data retrieved from [13], wherein only two parameters were considered, which were the total resistance and the dynamic trim angle. Since the total resistance values in the proposed reference were reported in the form of the total resistance coefficient, it is worth mentioning that the values taken from the reference were reformed to give the final total resistance corresponding to the equation: $R_T = 0.5\rho S V^2 C_T$, where R_T represents the total resistance in N, ρ stands for the water density in kg/m^3, S represents the wetted surface area in m^2, V is the boat speed in m/s and, finally, C_T is the total resistance coefficient reported in the reference study.

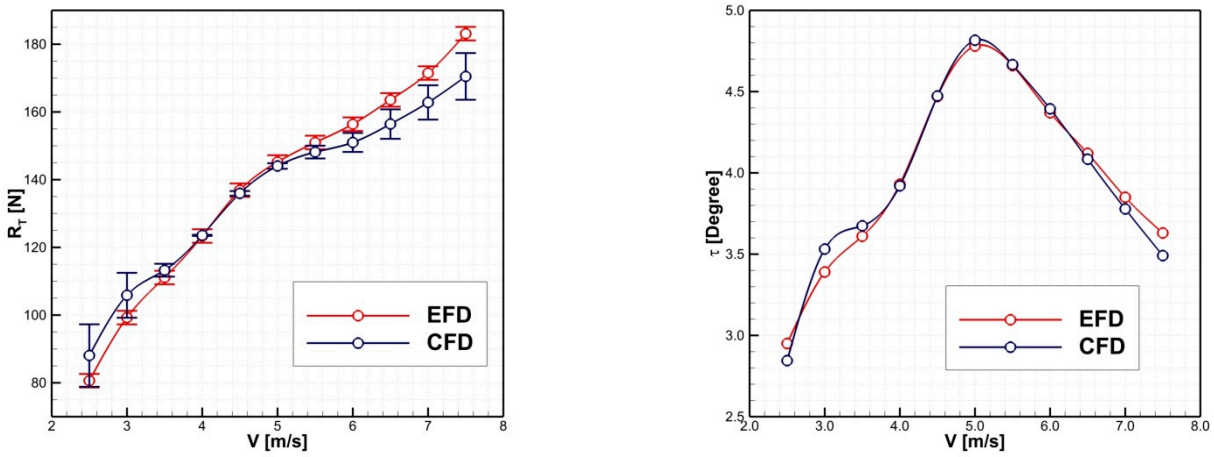

Figure 5. Total resistance and dynamic trim computed vs. experimental data reconstructed from Ref. [13].

It can be observed from the comparison between the CFD and EFD results that the errors are significant on both ends of the speed range. The maximum error occurs at the lowest speeds, while the high-speed range also results in perceptible errors. On the other hand, the errors are highly insignificant within the mid-speed range. This complies with the theoretical approach, wherein it is common in numerical simulations that the errors are significant at the lower speeds due to the lack of consistency in the numerical model from the cell-size point of view compared to the ship speed. This might result in a misleading motion prediction, as is the case in the obtained results here from the trim motion point of view, which possibly triggers a chain reaction with the total-wetted-surface-area prediction that makes an important factor in the total resistance equation. On the other hand, the discrepancies obtained at the high-speed ranges require more investigation. Possibly, the deviation from the EFD data is related to the under-predicted trim, which may affect the computed total resistance, as previously indicated. A finer grid and time step might contribute to the solution for this problem, as it will be observed in the verification section. Overall, if the criteria to be taken into consideration in the following study are regarded to the drag and lifting forces, it can be observed that the resistance prediction is within a reasonable level, wherein the average absolute error value is less than 4%, a value that is considered more than acceptable for resistance simulations.

4.1.2. Verification

A systematic verification procedure is performed in order to assess the numerical errors through grid- and time-step-convergence tests, based on the generalized Richardson Extrapolation (RE) method that is explained in detail in [44,45]. First, the verification study is applied to assess the numerical uncertainty U_{SN}, which can be expressed as

$$U_{SN} = \sqrt{U_I^2 + U_G^2 + U_T^2 + U_P^2} \tag{4}$$

where U_I represents the iterative uncertainties, U_G represents for the grid uncertainties, U_T stands for the time-step uncertainty and, finally, U_P stands for any other parameter.

The verification procedures start with the convergence study based on the convergence ratio that can be estimated based on the equation

$$R_k = \varepsilon_{k,21} / \varepsilon_{k,32} \tag{5}$$

According to the ITTC guidelines presented in [44], Equation (5) imposes three different conditions such that

i Monotonic convergence: $0 < R_k < 1$;

ii Oscillatory convergence: $R_k < 0$, $|R_k| < 1$;
iii Divergence: $R_k > 1$.

If a monotonic convergence is achieved, the RE error δ_{RE} can be estimated based on the refinement ratio r_k and the order of accuracy p_k according to Equations (6,7)

$$\delta_{RE} = \left(\frac{\varepsilon_{k,21}}{{r_k}^{p_k} - 1} \right) \tag{6}$$

while,

$$p_i = \frac{ln(\varepsilon_{k,32}/\varepsilon_{k,21})}{ln(r_k)} \tag{7}$$

For the second condition, if an oscillatory convergence is achieved, the uncertainty is estimated using the lower and upper values of oscillation, S_L and S_U, respectively, such that

$$U_k = \frac{1}{2}(S_U - S_L) \tag{8}$$

and, finally, if a divergence condition is achieved, this means that the errors and uncertainties cannot be estimated.

On the other hand, the validation is accomplished through comparing the estimated error E with the validation uncertainties U_V based on the data uncertainty U_D, according to the equation

$$U_V = \sqrt{U_{SN}^2 + U_D^2} \tag{9}$$

When $|E|$ is within U_V range, solutions are validated at the U_V interval; otherwise, the results might be validated at another required validation level U_{req}; else, the results are not validated.

Quantitatively, the results for the grid- and time-step-convergence studies are tabulated in Tables 4 and 5, respectively, calculated for only three speeds, corresponding to V = 2.5, 5.0 and 7.5 m/s. In both convergence studies, a monotonic convergence is achieved for the boat speeds V = 2.5 and 7.5 m/s, while at V = 5.0 m/s, an oscillatory convergence is achieved. It is also clear that the grid influence on the solution is very significant, while the time-step influence is almost insignificant, as Table 5 bears out, which means that the initial time step is sufficient for obtaining good results. Figure 6 shows the error changes based on both grid- and time-step-convergence studies.

Table 4. Results for grid-convergence study.

Grid-Convergence Parameters	V (m/s)	r_G	R_G	p_G	p_{th}	U_G%D
Value	2.5	1.65	0.31	2.39	2.0	8.91
	5.0		−0.19	N.A.		4.42
	7.5		0.51	1.33		3.15

Table 5. Results for time-step-convergence study.

Time-Step-Convergence Parameters	V (m/s)	r_T	R_T	p_T	p_{th}	U_T%D
Value	2.5	2.0	0.08	3.70	2.0	0.3
	5.0		−0.9	N.A.		0.25
	7.5		0.58	N.A.		0.12

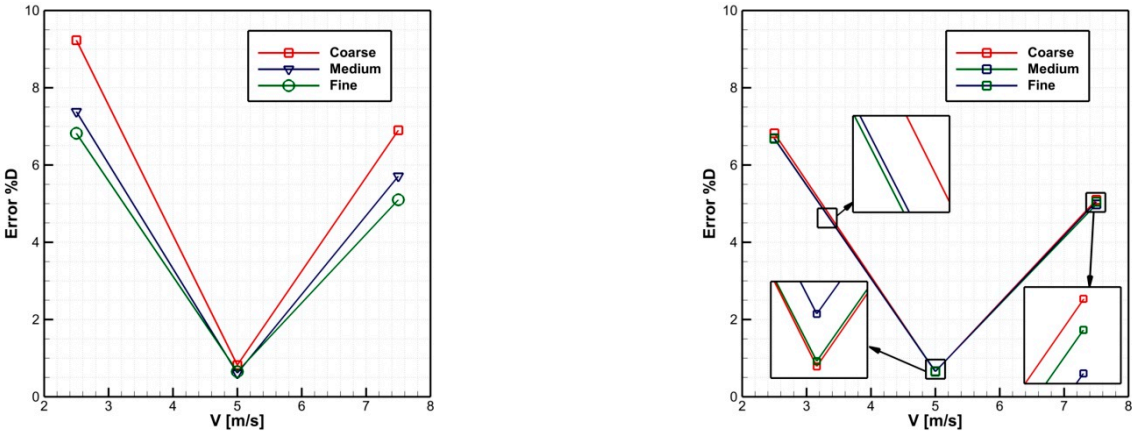

Figure 6. Numerical errors for: (**a**) grid- and (**b**) time-step-convergence studies.

The validation of the numerical errors is presented in Table 6, showing that the coarsest grid results are not validated at the U_V level for low- and high-speed ranges; however, for the medium-speed range, all the results were validated at the validation uncertainty level. The medium and fine grid results are within the validation level of uncertainty. For this reason, a fine grid is necessary to maintain a low level of numerical errors. Consequently, the finest grid parameters will be applied to generate the grids used for the following study.

Table 6. Results for validation study.

Validation Parameters	V (m/s)	U_{SN}	U_D	U_V
Value	2.5	8.91	0.1	8.91
	5.0	4.42		4.43
	7.5	3.15		3.15

As for the verification study of the optimized hull, the effect of changing the grid and time step was insignificant and did not have any influence on the predicted resistance values during the numerical simulation. All the differences between the errors are less than 1%, which makes the study grid- and time-step-independent. This may require further investigation, since it cannot be considered as a general case; however, it may reflect the proper choice of the mesh size and also the time step.

4.2. The Comparative Study Results

4.2.1. Tunnel Shape Improvement

The design of the tunnel entrance impacts the transition of the water flow from the hull bottom up into the tunnel. This transition length must not be excessive to a limit that results in a significant loss of buoyancy and dynamic lift near the stern of the vessel. In most cases, the design of a tunnel entrance is analogous to that of waterjet inlet design [46]. However, the loss of planing surface and interior volume may produce a reduction in buoyancy and dynamic lift while underway.

The slope of the tunnel roof must be designed to avoid flow separation. It is recommended that the slope of the tunnel roof not exceeds a 15° change relative to the hull bottom for speeds of Fr < 2.5 and that the slope be less for higher speeds. The entrance should not be wider than the width of the tunnel at the propeller plane [47].

Analyzing the pressure distribution on the bottom of the version V1 of the boat, a spot of significant negative pressure appears on the front of the tunnel entrance, which is susceptible to flow detachment. The detachment of the flow may lead to nonhomogeneous velocity fields in the propeller disc with a direct effect on the propeller efficiency. Extending the length of the tunnel by 23%, the slope of the tunnel was reduced from 9° to 5°. A

comparison of the pressure distribution for the initial shape of the tunnel (V1) and the improved one (V6) is plotted in Figure 7 for speeds of 32, 36 and 40 knots. Figure 8 reveals that the lower-pressure area in front of the tunnel entrance has been successfully diminished, but also that higher-pressure area on the tunnel has slightly been decreased.

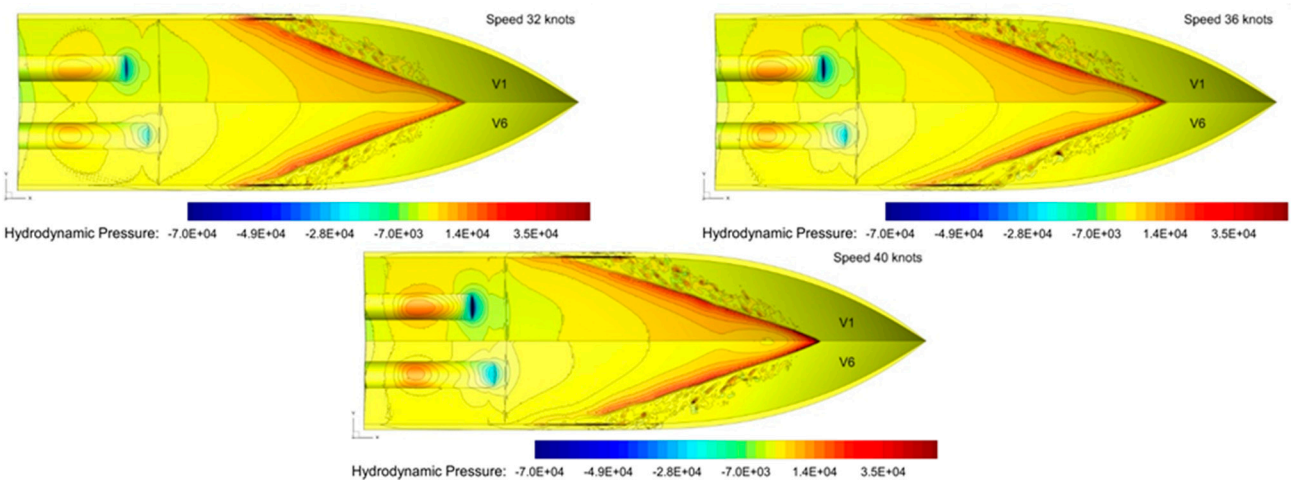

Figure 7. Comparison of pressure distribution on the hull bottom for V1 and V6 at different speeds.

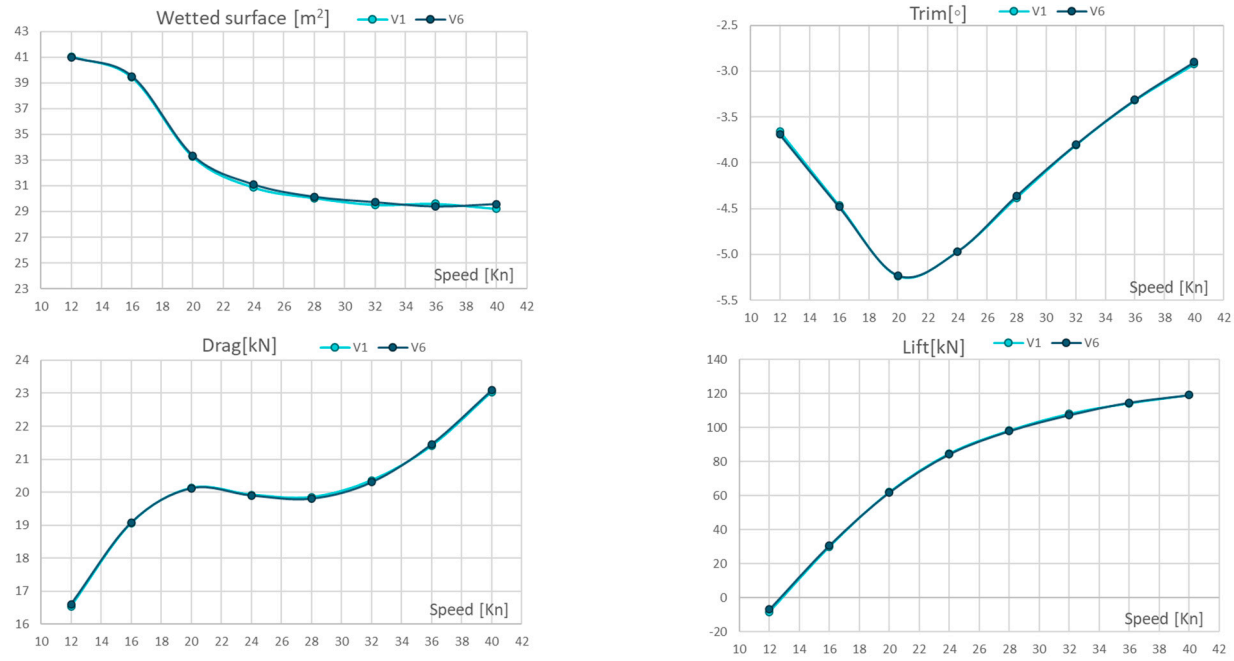

Figure 8. Variation of main computed parameters with respect to boat speed.

The results of the computations are presented in Figure 8, wherein the variation of wetted surface, drag, lift, trim and sinkage are plotted functions of speed.

In Table 7 are presented the relative variation of the wetted surface, drag, lift and trim, which are calculated based on the reference values obtained in the initial hull version V1. As long as most of the difference was less than 1% on all global parameters, one may say that no significant improvement has been added by the tunnel modification. On the other hand, comparing the lift force acting only on each tunnel surface, it has been found that lift decreased by about 21–22% for version V6 (Table 8).

Table 7. Relative variation/difference of global quantities.

Speed (kn)	Wetted Surface	Trim	Lift	Drag	Pressure Drag	Viscous Drag
12	−0.15%	0.95%	0.91%	0.40%	0.38%	0.55%
16	0.26%	0.30%	2.65%	0.09%	0.07%	0.28%
20	0.31%	−0.18%	−0.31%	−0.03%	−0.15%	0.48%
24	0.75%	−0.05%	−0.44%	−0.11%	−0.24%	0.28%
28	0.30%	−0.51%	−0.34%	−0.23%	−0.51%	0.31%
32	0.67%	−0.18%	−0.70%	−0.28%	−0.50%	0.12%
36	−0.73%	−0.24%	0.30%	0.24%	−0.25%	0.19%
40	1.28%	−0.82%	0.02%	0.24%	−0.29%	0.69%

Table 8. Lift computed on tunnel surface.

Speed (kn)	V1	V6	
	Lift tunnel	Lift tunnel	Diff. lift%
32	2.767	2.161	−21.90%
36	3.918	3.091	−21.11%
40	5.129	4.019	−21.64%

4.2.2. The Effect of Spray Rail Width

High-speed craft generates spray, generally with impact pressure at the bow region. The direction of the spray will influence the position of the maximum pressure point. The form and nature of the spray will vary with the craft speed, trim and hull characteristics. The spray rail/hard chines are fundamental features to separate the flow and to generate lift force and dynamic trim on the body. However, the spray gives contribution to the pressure on the body, especially at higher speeds.

To investigate the effects of the spray rail (SR) width on the hull hydrodynamics, the width of the initial SR (0.11 m, V6) has been extended to 0.15 m (V4) and 0.19 (V3). A slightly transversal reverse angle of the SR could be seen for version V3 and V4. It should be mentioned that the extension of the SR leads to a modification of the deadrise angle as presented in Table 9. For illustration purposes, four sections at different longitudinal distances are depicted in Figure 9 to show how the three hulls differ geometrically.

Table 9. Lift computed on tunnel surface.

Position	Deadrise Angle (°)		
	V3	V4	V6
Stern	17.3	16.9	17.9
Midship	21.96	21.48	19.73

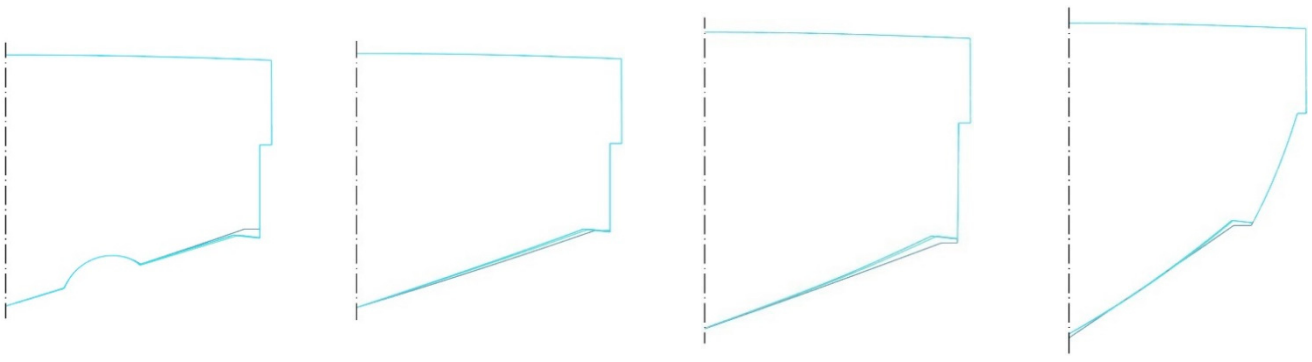

Figure 9. Transversal sections at different longitudinal distances for versions V3, V4 and V6.

The results of the computations carried out for the V3, V4 and V6 are presented in Figure 10, wherein the variation of wetted surface, trim, drag and lift is plotted as a function of speed. V6 has the lower wetted surface, but also the higher trim angle for all the speeds. In terms of ship resistance, the lower drag has been shown by the V4 for the speed range of 16 to 36 kn, but for the higher speed computed, V6 experienced the minimum resistance. Analyzing the drag curves, one may see that a change in slope of the V4 curve starts at a speed of 32 kn. No significant differences in lift global values have been observed. In order to further analyze the hull-shape effect on boat hydrodynamic performances, Figure 11 shows the distribution of pressure drag, viscous drag and lift in 20 sections along the hull. The pressure resistance distribution along the hull revealed an efficient bow shape for V6 in comparison with the other two versions, as the pressure drag corresponding to X in range of 7 to 9 m is significantly lower, Figure 11 (top). If the lift distribution is assessed, all versions show a lift local maximum at X = 0.5 m, but a second local maximum for V3 and V4 appears at about X = 4 m and for V6 is shifted to X = 5.5 m. Analyzing the distribution of viscous forces, V6 shows lower friction on the bow area from X = 6 to 9 m.

In order to quantify the contribution of the SR on the total hull lift, the lift generated by the SR has been extracted for each version for speeds of 32, 36 and 40 kn (Table 10). For V6, SR brings about 5%, V3 about 11% and V4 about 7% of total hull lift. On the other hand, the relative differences between the lift produced by the SRs of V3 and V4 compared with the lift generated by V6 SR (see Table 11) show a significant increase in the lift brought by the extension of the SR width.

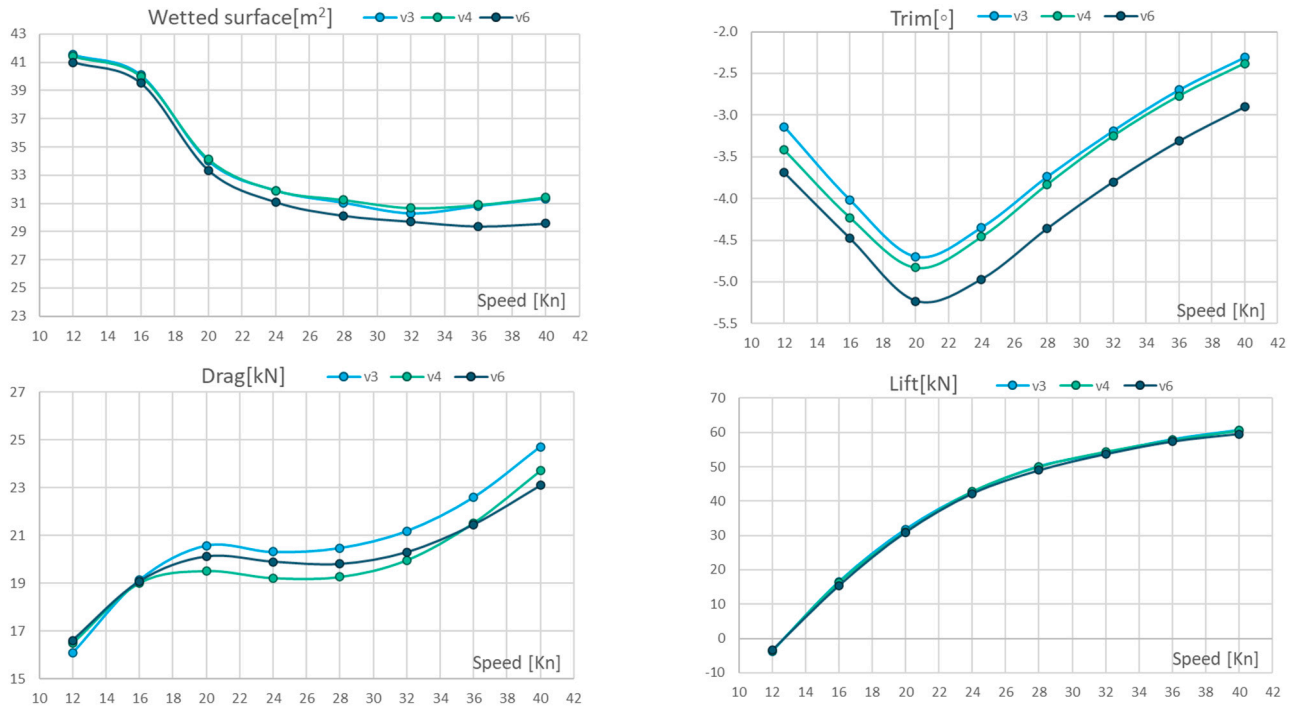

Figure 10. Variation of main computed parameters for V3, V4 and V6.

Table 10. Lift computed on the hull and SR.

Speed (kn)	Lift SR	Lift Hull		Lift SR	Lift Hull		Lift SR	Lift Hull	
	V6	V6	SR vs. Hull	V3	V3	SR vs. Hull	V4	V4	SR vs. Hull
32	2.72	53.697	5.06%	6.156	53.994	11.40%	3.949	54.42	7.26%
36	3.07	57.359	5.35%	5.964	57.948	10.29%	4.229	57.818	7.31%
40	2.76	59.573	4.63%	7.041	60.631	11.61%	5.161	60.544	8.52%

Table 11. Comparison of lift computed on SR.

Speed (kn)	Lift SR V6	Lift SR V3	Lift SR V3 vs V6	Lift SR V4	Lift SR V4 vs. V6
32	2.72	6.156	126.4%	3.949	45.24%
36	3.07	5.964	94.3%	4.229	37.80%
40	2.76	7.041	155.1%	5.161	86.99%

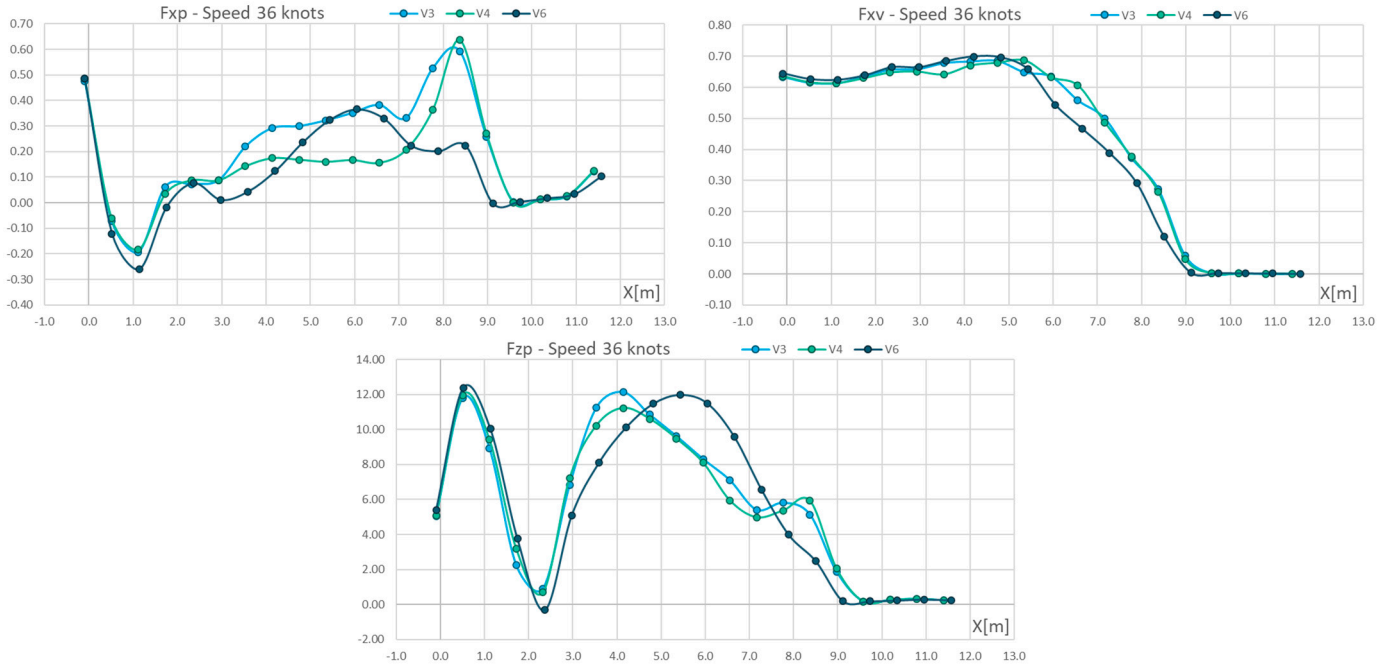

Figure 11. Comparison of Fxp, Fxv and Fzp along the hull for V3, V4 and V6.

Taking into consideration that the most efficient solutions in terms of drag are V6 and V4, in the following, more comparisons between the obtained results for those cases are added. Relative variation of the wetted surface, drag, lift and trim, calculated considering as reference the results obtained for initial hull version, V6, are presented in Table 12. The comparison proves a reduction in the total drag for the speed range of 12 to 32 kn and a slight increase in the lift. The drag reduction is based on the decrease of pressure resistance. One important aspect for this particular case is the propeller shaft inclination of 13°. Moreover, the boat dynamic trim contributes to the increase of the shaft angle, which by superposing effects can reach very high inclination with negative influence on the propeller efficiency. So, the decrease of trim angle by up to 17% experienced by V4 should be seen as a benefit in terms of propulsion improvement.

Table 12. Relative difference of global quantities: V4 vs. V6.

Speed (kn)	Wetted Surface	Trim	Lift	Drag	Pressure Drag	Viscous Drag
12	1.02%	−7.32%	−187%	−0.69%	−0.85%	0.44%
16	1.21%	−5.58%	6.06%	−0.34%	−0.48%	0.41%
20	2.34%	−7.65%	0.58%	−2.97%	−3.71%	0.26%
24	2.64%	−10.26%	1.50%	−3.41%	−5.38%	2.51%
28	3.72%	−12.16%	2.17%	−2.69%	−5.61%	3.33%
32	3.23%	−14.47%	1.35%	−1.63%	−5.00%	3.26%
36	5.17%	−16.31%	0.80%	0.34%	−3.54%	4.47%
40	6.29%	−17.93%	1.63%	2.68%	−0.86%	5.62%

In order to achieve a better understanding of the relation between hull shape, pressure and forces distribution along the boat length, Figure 6 bares the comparative results for V4 and V6 (Figure 12), at 36 and 40 kn.

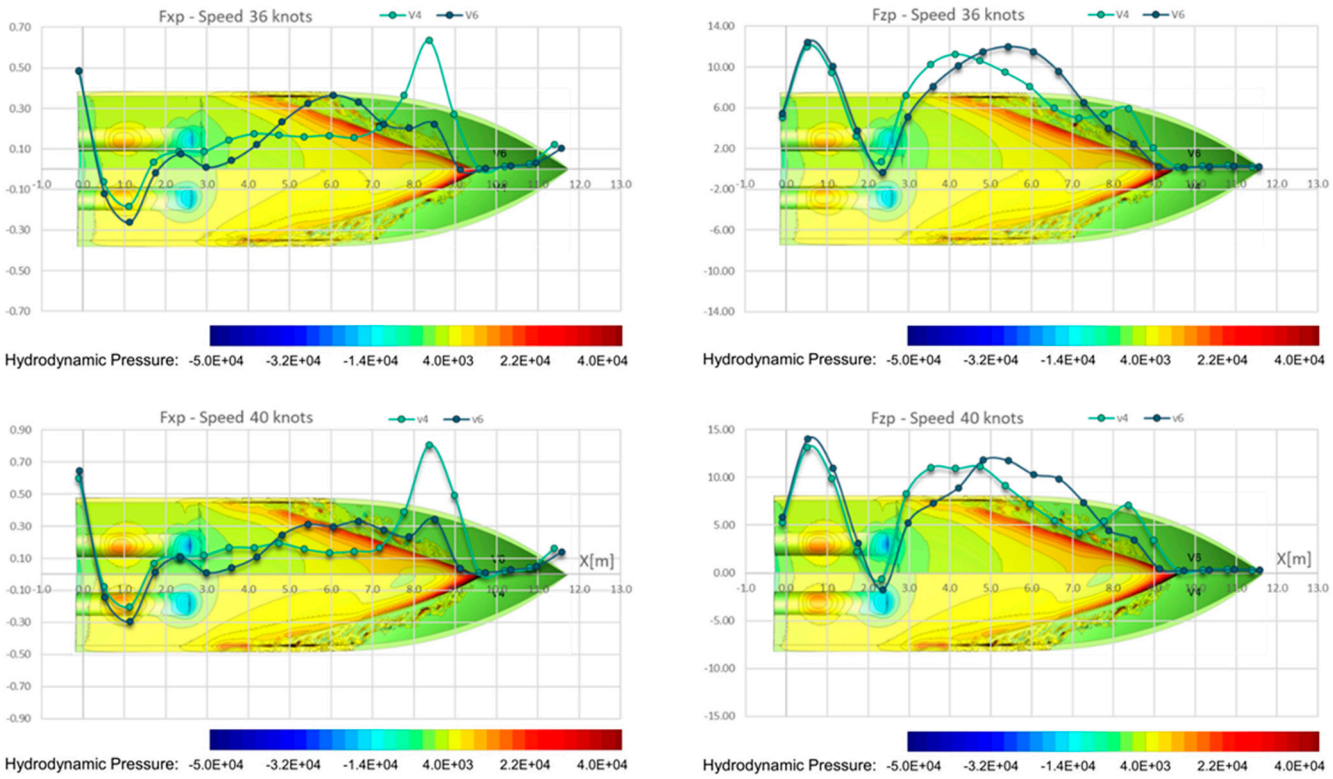

Figure 12. Forces and pressure distributions comparison for V4 and V6, at 36 and 40 kn.

4.2.3. The Effect of Whisker Rails

One Pair of Whisker Rails

Planing hulls use different geometric features to reduce the drag and increase the lift. Hydrodynamic pressure on the bottom of the hull is a significant factor that contributes to the lift of the hull. Whisker rails (WR) were designed to control the flow direction, increase the hydrodynamic lift on the hull and to reduce the trim angle. Usually, these are triangular protrusions which run dead straight when viewed from below and redirect the flow of water downward [3]. This increases the lift and reduces the wetted surface area.

The present section is focused on studying the effects of the whisker rails on the hydrodynamic performances of the planing boat. Two sets of computations have been performed considering the initial bare hull (V1) and the same hull equipped with one pair of whisker rails V2 (V1 + one pair of whisker rails). The results of the computations carried out for the V1 and V2 are presented in Figure 13, wherein the variation of wetted surface, trim, drag and lift are plotted as functions of speed. Results reveal that the wetted surface for speeds higher than 28 kn is lesser for the hull with whisker rails (V2), which leads to a reduction of the viscous resistance up to 4% (Table 13).

On the other hand, pressure resistance shows lower values all over the curve, which finally leads to a total resistance improvement of about 2% for a speed range of 20 to 40 kn. Another benefit of the whisker rails is the significant reduction in the trim, by 6 to 15%. Somehow unexpectedly, the total lift of the hull decreased to 4–8 % for the hull equipped with whisker rails. Most probably the reduction is caused by the lower trim angles.

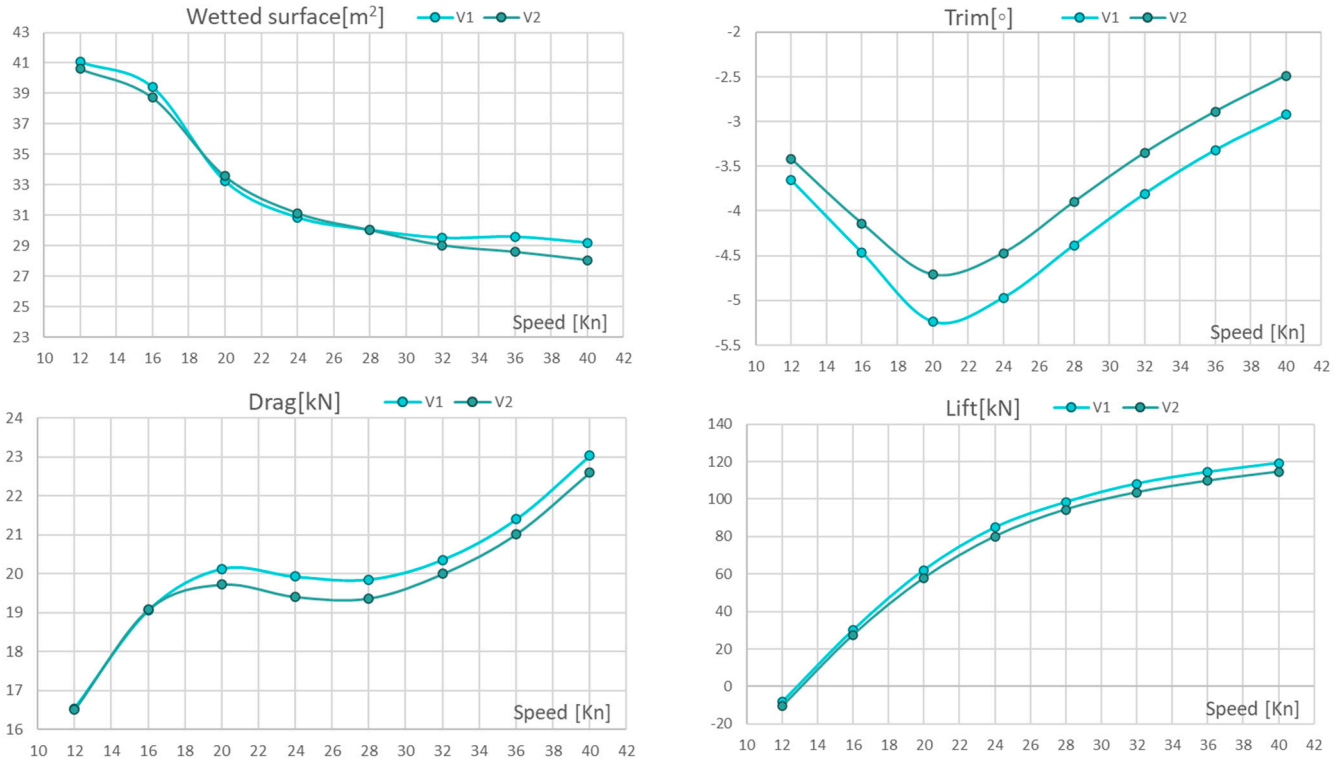

Figure 13. Variation of main computed parameters for V1 and V2.

Table 13. Relative difference of global quantities: V1 vs. V2.

Speed (kn)	Wetted Surface	Trim	Lift	Drag	Pressure Drag	Viscous Drag
12	−1.07%	−6.44%	27.3%	−0.18%	−0.30%	0.78%
16	−1.73%	−7.32%	−8.38%	0.09%	−0.07%	1.10%
20	0.95%	−10.11%	−6.81%	−2.01%	−2.97%	2.18%
24	0.93%	−10.10%	−5.56%	−2.60%	−4.02%	1.70%
28	−0.01%	−11.01%	−3.96%	−2.43%	−3.73%	0.25%
32	−1.62%	−12.00%	−4.28%	−1.78%	−2.50%	−1.18%
36	−3.32%	−12.90%	−4.08%	−1.81%	−1.19%	−3.05%
40	−3.87%	−14.84%	−3.88%	−1.93%	0.76%	−4.18%

Continuing the investigation on lift, the hydrodynamic pressure integrated on the SR only showed a significant lift decrease (Table 14) for the case with whisker rails. It seems that the lift force is shared between SR and whisker rails. When the contribution of SR and WR on total hull lift is checked, the values bared in the Table 15 show that the effects of SR and WR are almost similar.

Table 14. Comparison of lift computed on SR.

Speed (kn)	Lift SR	Lift SR	Lift SR
	V1	V2	V1 vs. V2
32	2.97	1.99	−32.6%
36	2.90	1.90	−34.7%
40	2.82	2.15	−23.9%

Table 15. Comparison of lift computed on SR.

Speed (kn)	Lift Hull	Lift SR	Lift SR	Lift Hull	Lift SR	Lift Whisker	Lift SR	Lift Whisker	Lift Hull
	V1	V1	%	V2	V2	V2	%	%	V1
32	54.076	2.965	5.48%	51.762	1.998	1.912	3.86%	3.69%	54.076
36	57.189	2.903	5.08%	54.853	1.896	1.819	3.46%	3.32%	57.189
40	59.559	2.817	4.73%	57.248	2.145	1.844	3.75%	3.22%	59.559

In order to further analyze the hull shape effect on boat hydrodynamic performances, Figure 14 shows the distribution of pressure drag, viscous drag and lift in 20 sections along the hull, but also a comparison of the pressure on hull, with and without whisker rails. The distribution of the pressure resistance along the hull revealed an efficient bow shape for V1 in comparison with V2, as the pressure drag (Fxp) corresponding to X in the range from 7 to 9.5 m is significantly lower (Figure 14 (top)). It seems that the bow shape of V1 shows a positive effect in terms of viscous resistance at X from 7 to 9 m, then the WR changes the friction distribution, which leads to a reduction in the viscous resistance at X from 4 to 7.5 m. If the lift distribution is assessed, adding a pair of whiskers rails is not necessarily increasing the lift in the area where WR is located, but a uniform distribution of lift (X = 4.5–8.5 m) has been noticed.

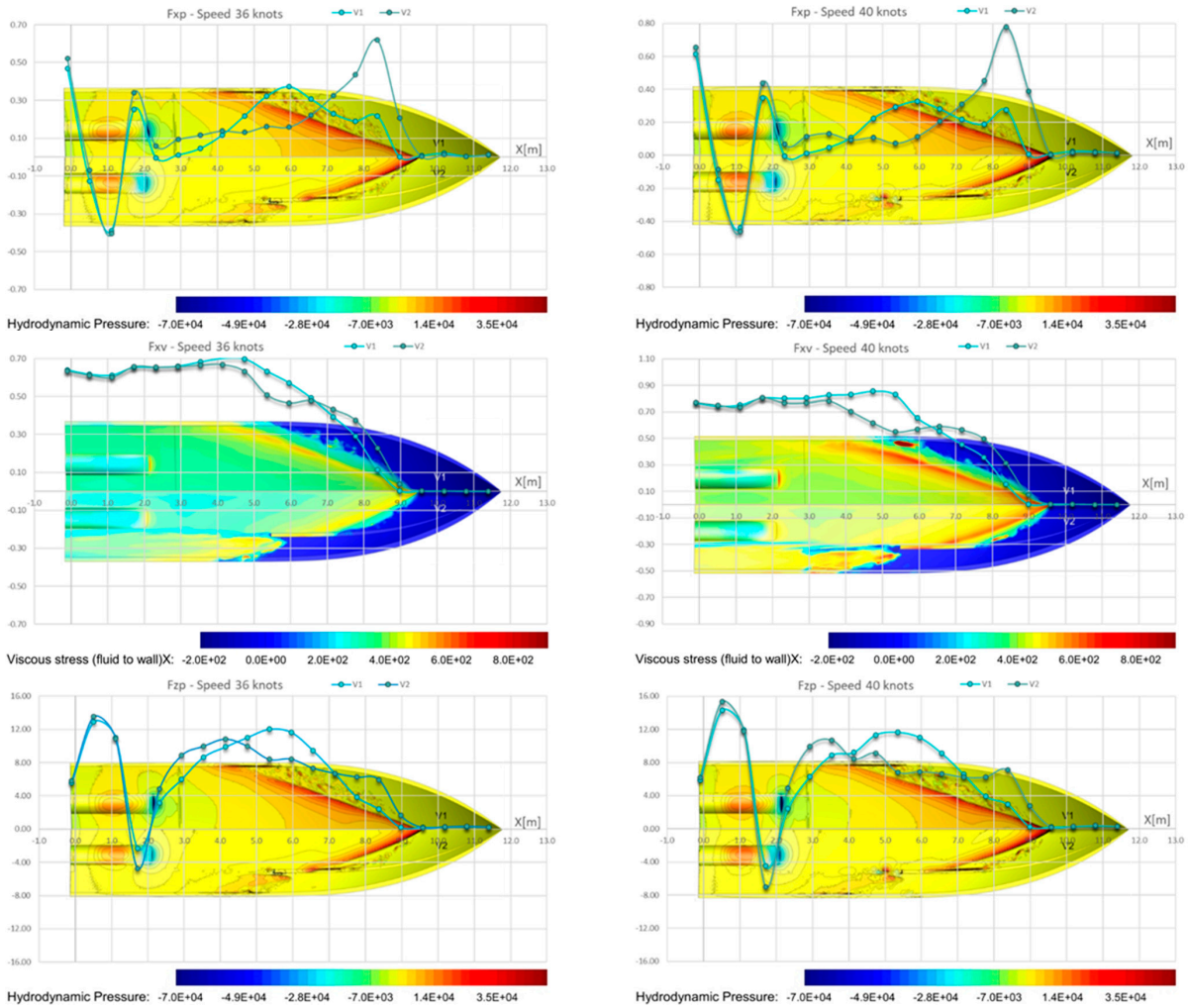

Figure 14. Forces and pressure distributions comparison for V1 and V2, at 36 and 40 kn.

Further analysis using the volume fraction combined with an iso-surface of the air–water interface gives further insight. The WR clearly separates the flow from the hull surface, as shown by the bottom half of the Figure 15. This separation appears to entrain air outside of the WR, shown by the streak along the hull in the Figure 15 (bottom). The air seems to not reach the propeller area in this case, but this most probably will happen when the flow upstream the propeller is affected by the suction of the propeller. Comparing the pictures for different speeds, a faster dissipation of the aeration appears at lower speeds.

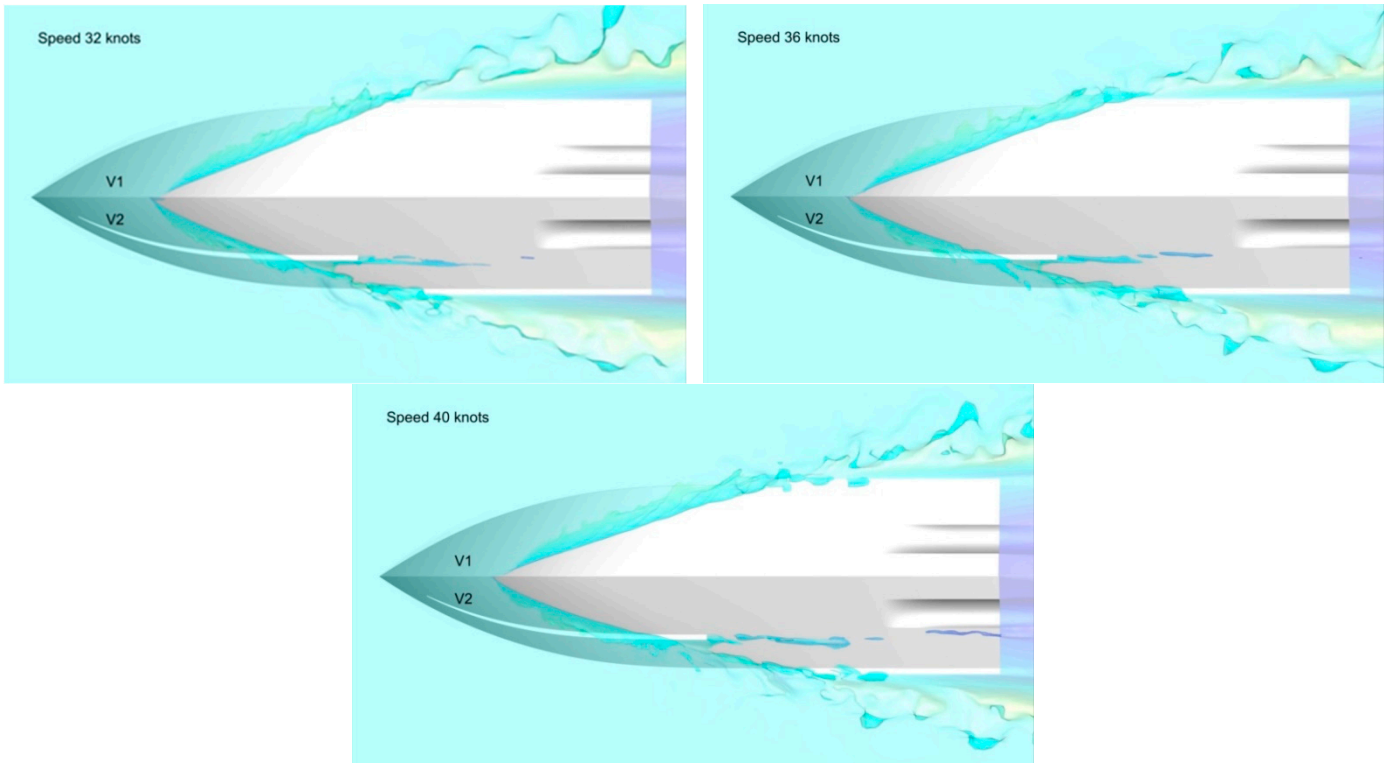

Figure 15. Comparison of free-surface and air-pocket development for V1 and V2, at 32, 36 and 40 kn.

Two Pairs of Whiskers Rails

To further investigate the effects of the whisker rails on the hydrodynamic performances of the planing boat, two pairs of WR have been mounted on the bare hull of V4. Moreover, the shape of the WR has been improved at leading and trailing edge. In the same manner, the results of the computations carried out for the V4 (bare hull) and V7 (V4 + 2 pair of WR) are presented in Figure 16, wherein the variation of wetted surface, trim, drag and lift are plotted as a function of speed. Results reveal that the wetted surface for speeds higher than 24 kn decreases significantly for the hull with whisker rails (V7), with direct effects on the reduction of the viscous resistance by up to 17.6% (Table 16). The area of lower friction may be clearly seen in the Figure 17 (2nd and 4th picture), where friction distribution on the hulls V4 and V7 are compared. The same trend is shown by the Fxv distribution along the hull and major viscous drag reduction appears from section X = 4 m to section X = 8.5 m. On the other hand, pressure resistance shows a slight increase, of 0.67 to 1.80%, all over the curve. Finally, mainly due to the friction reduction, a maximum total resistance improvement of about 9 % at the highest speed has been reached. The total lift of the hull decreased by 3–6.5 % for the hull equipped with whisker rails. This is most probably, in this case, because of the aeration effect, a phenomenon that is clearly described by the pictures in Figure 18.

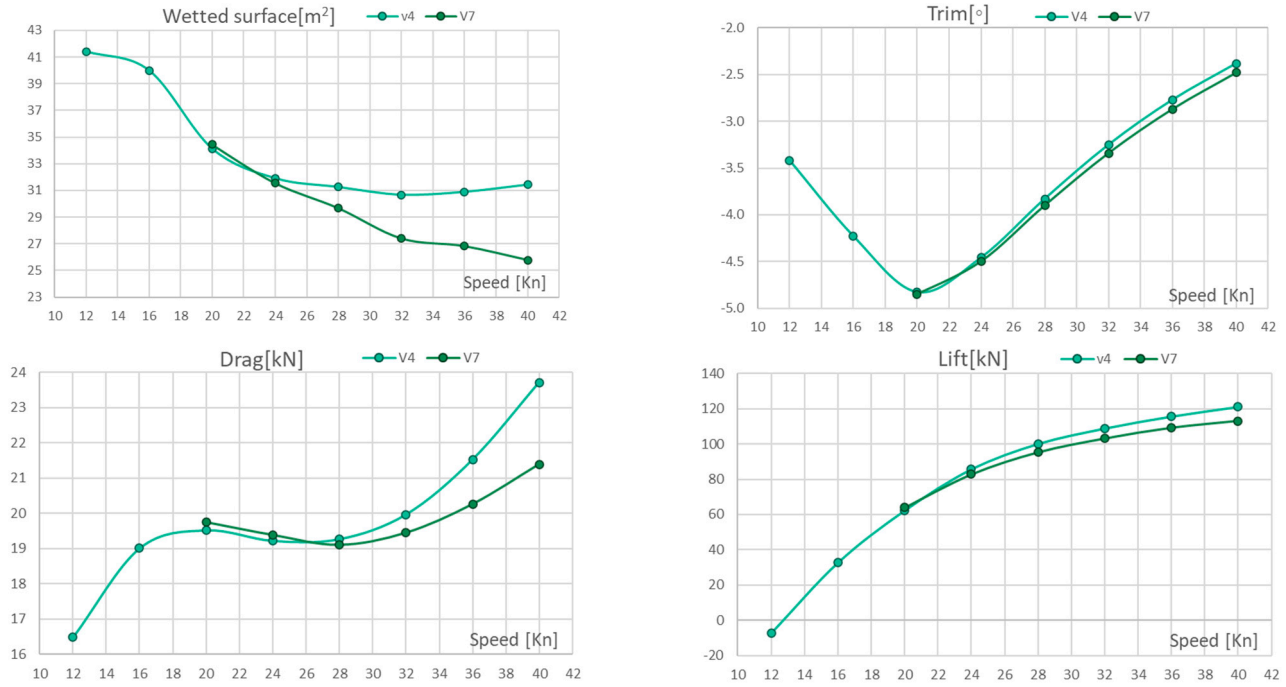

Figure 16. Variation of main computed parameters for V4 and V7.

Table 16. Relative difference of global quantities: V4 vs V7.

Speed (kn)	Wetted Surface	Trim	Lift	Drag	Pressure Drag	Viscous Drag
20	0.94%	0.41%	2.70%	1.20%	1.08%	1.69%
24	−1.13%	0.90%	−3.30%	0.88%	1.19%	0.08%
28	−5.05%	1.83%	−4.76%	−0.83%	1.15%	−4.54%
32	−10.69%	2.77%	−5.19%	−2.57%	1.45%	−7.97%
36	−13.20%	3.61%	−5.50%	−5.85%	1.80%	−13.03%
40	−18.00%	4.20%	−6.53%	−9.76%	0.67%	−17.60%

Further investigating the lift, the hydrodynamic pressure integrated on the SR only showed a significant lift decrease (Table 16) for the case with whisker rails (V7). It seems that the lift force is shared between SR and whisker rails. When the contribution of SR and WRS on total hull lift is checked, the values bared in Tables 17 and 18 show the contribution of SR and each WR on the total lift.

Table 17. Comparison of lift computed on SR.

Speed (kn)	Lift SR	Lift SR	Lift SR
	V4	V7	V4 vs. V7
32	3.95	3.57	−9.67%
36	4.23	3.64	−13.86%
40	5.16	3.70	−28.35%

Table 18. Comparison of lift computed on SR and WR.

Speed (kn)	Lift Hull	Lift SR	Lift SR	Lift Hull	Lift SR	Lift WR1	Lift WR2	Lift SR	Lift WR1	Lift WR2
	V4	V4	%	V7	V7	V7	V7	%	%	%
32	54.42	3.95	5.48%	51.597	3.57	2.23	1.99	6.91%	4.32%	3.86%
36	57.82	4.23	5.08%	54.637	3.64	2.34	2.20	6.67%	4.28%	4.02%
40	60.54	5.16	4.73%	56.591	3.70	2.49	2.40	6.53%	4.40%	4.24%

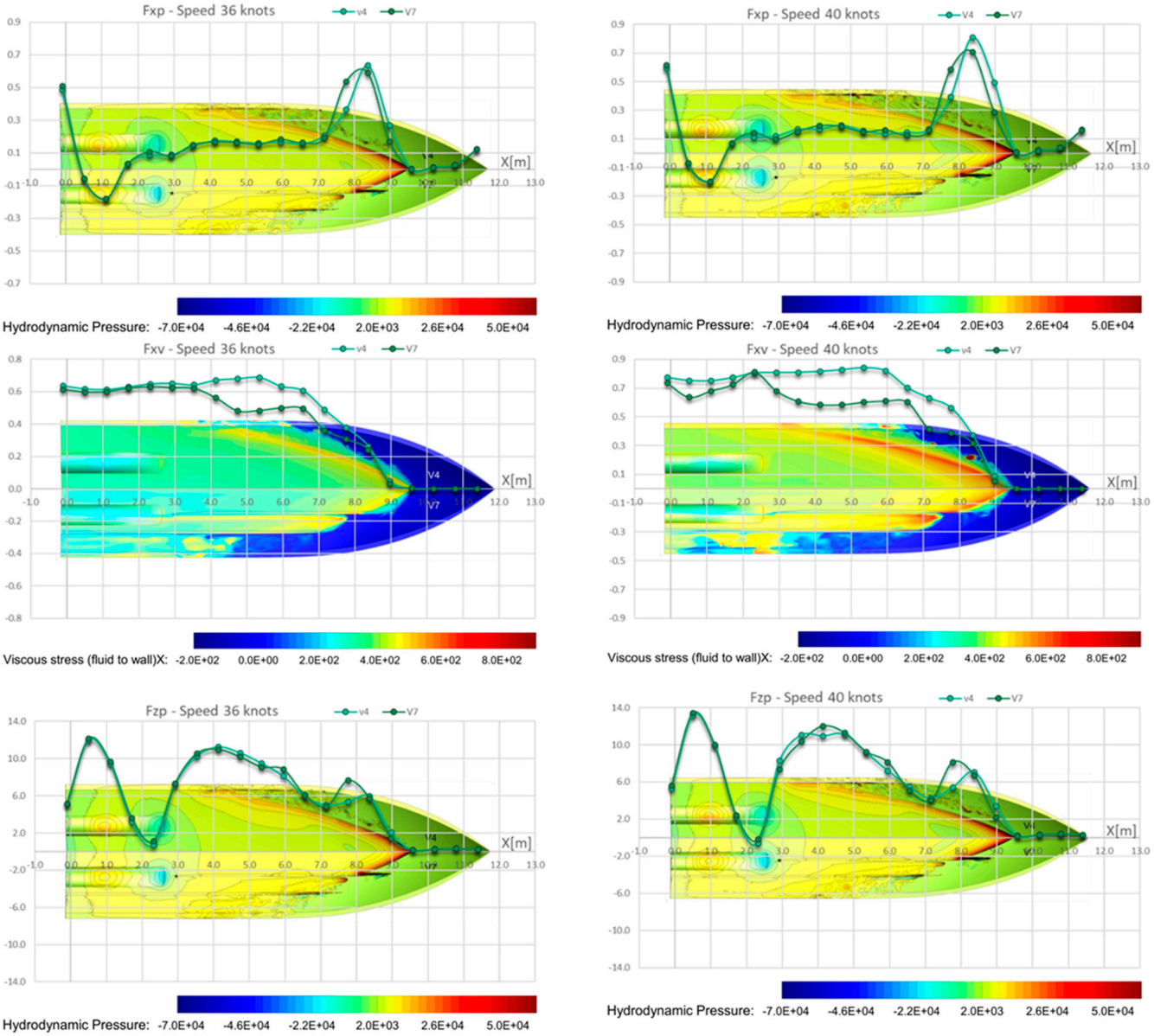

Figure 17. Forces and pressure distributions comparison for V4 and V7, at 36 and 40 kn.

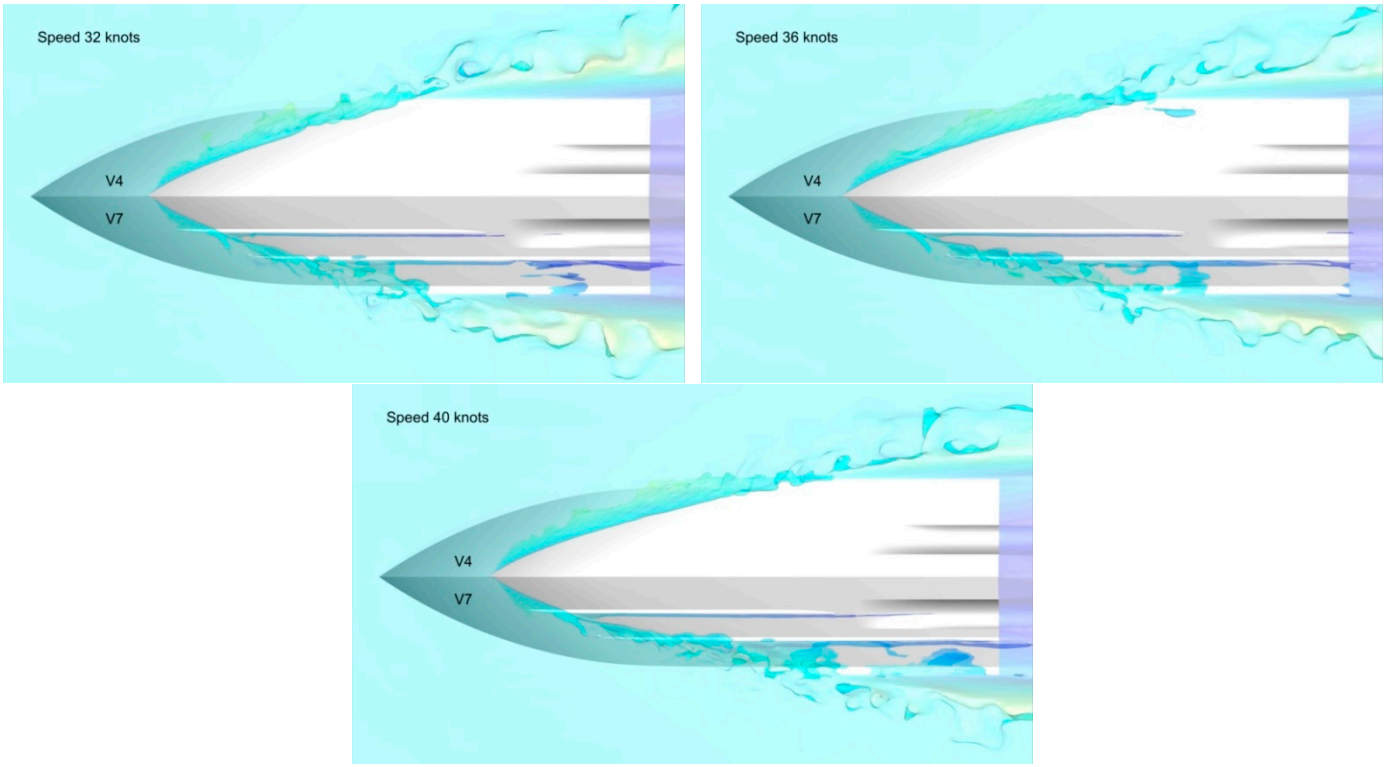

Figure 18. Comparison of free-surface and air-pocket development for V4 and V7, at 32, 36 and 40 kn.

4.2.4. The Effect LCG Shift

Another approach to reduce the ship resistance of a planing boat is to modify the longitudinal position of the center of gravity. Considering the design constraints, the LCG was moved by 0.2 m toward transom for the hull version V4. Two sets of computations have been performed considering the bare hull (V4) with LCG = 4.157 m and the same hull with LCG = 3.957 m (V5). The results of the computations carried out for the V4 and V5 are presented in Figure 19, wherein the variation of wetted surface, trim, drag and lift are plotted as functions of speed. Results reveal that the wetted surface is lower for the V5, which leads to a reduction in the viscous resistance of up to 5% (Table 19). On the other hand, pressure resistance shows lower values for speeds higher than 24 knots, which finally leads total resistance improvement up to 3.7%. It is worth mentioning that the obtained results show a significant trim angle at lower speed. This should be taken into consideration because this trim angle is expected to increase when the shaft is added to the boat and the propeller starts to produce thrust because the significant inclination angle of the shaft will contribute in increasing the trim.

Table 19. Comparison of lift computed on SR.

Speed (kn)	Wetted Surface	Trim	Lift	Drag	Pressure Drag	Viscous Drag
12	−0.87%	24.56%	−80.92%	4.97%	5.68%	−0.55%
16	−5.15%	21.51%	19.80%	2.66%	3.80%	−3.63%
20	−6.44%	13.46%	11.85%	1.12%	2.73%	−5.63%
24	−5.08%	8.30%	5.83%	−0.46%	1.00%	−4.49%
28	−4.61%	6.27%	5.06%	−1.62%	−0.67%	−3.41%
32	−3.85%	5.23%	1.94%	−2.78%	−1.84%	−4.04%
36	−4.01%	4.69%	1.76%	−3.51%	−2.90%	−4.12%
40	−4.33%	3.78%	1.00%	−3.76%	−4.03%	−3.48%

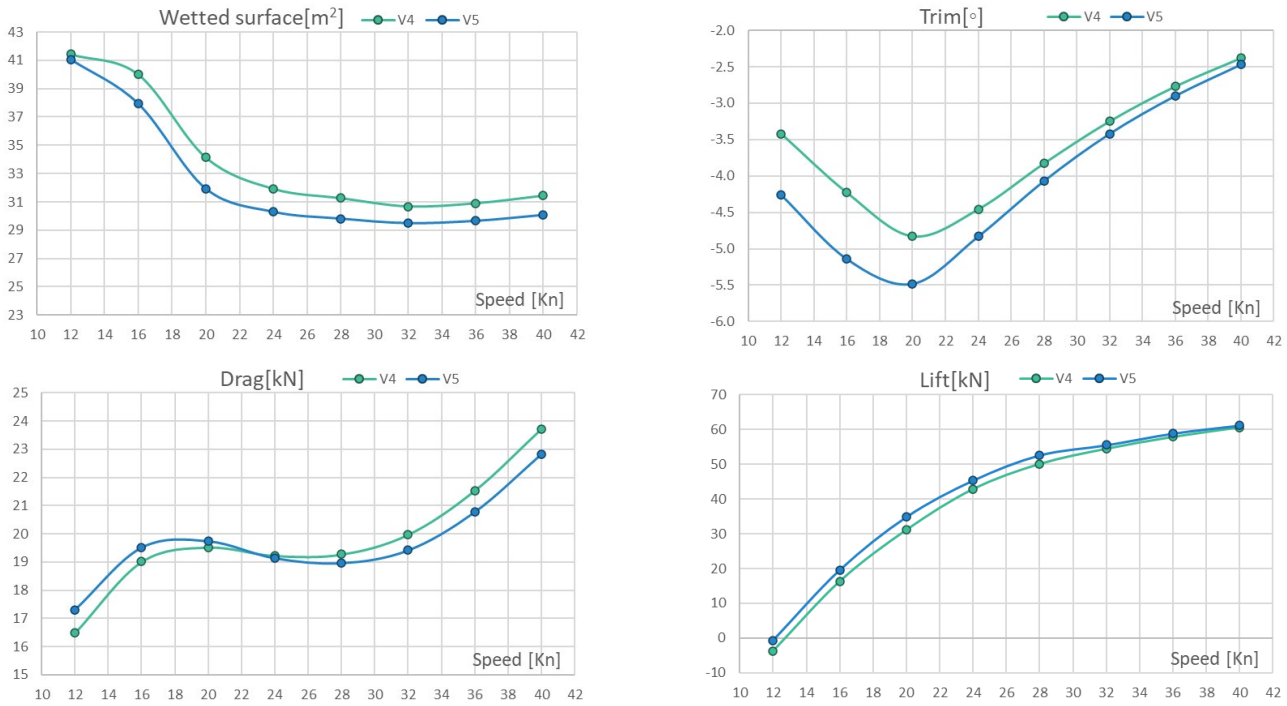

Figure 19. Variation of main computed parameters for V4 and V5.

5. Conclusions

The CFD simulation of the hydrodynamic performance of a planing hull, taking into consideration several geometrical parameters modifications, such as the tunnel configuration, whiskers and spray rails, while studying their influence on the hydrodynamic parameters of the planing hull, was presented, taking into consideration two various stages. The first is to validate the capability of the CFD to accurately capture the basic hydrodynamic parameters of concern. This was achieved by performing a separate analysis for validating the numerically obtained results based on the EFD data provided in [13]. This study also included a verification test to estimate the numerical errors and uncertainties, while also establishing a base for the proper choice of the grid cell size and time step. The second stage is to perform the comparative study for the hull under investigation, based on the information obtained from the first stage. This study also included a verification test for estimating the numerical uncertainties associated in the current study.

The verification and validation data for the first study were presented and were shown to have a proper agreement with the available experimental data in terms of resistance and trim angle. The verification study showed that the simulation was more dependent on the grid rather than the time step, wherein the influence of the time step changing was insignificant. Similarly for the comparative study, the verification test was concluded to be grid- and time-step-independent, a fact that reflects the proper choice of the grid cell size and time step for the simulation. However, the numerical parameters used for the simulation cannot be generalized from only a single study—further investigation is required. Still, as is well established in the CFD simulation, a proper combination between the time step and cell size can improve the quality of the numerical simulation and reduce the associated errors.

As for the comparative study, by quantitatively analyzing the variation in the global parameters, such as wetted surface, drag, lift, trim and sinkage, but also qualitatively investigation of the flow parameters, the following conclusions can be drawn:

1. Tunnel shape improvement has brought no significant positive effect on global quantities, considering that most of the difference was less than 1% for all global quantities. Even so, the main reason for the tunnel shape improvement has been to reduce the

spot of significant negative pressure on the front of the tunnel entrance, which is susceptible of flow detachment, which may lead to nonhomogeneous velocity fields in the propeller disc with direct effects on the propeller efficiency. The amelioration of the lower pressure area at the tunnel entrance can be checked in Figure 7.

2. To investigate the effects of the spray rail width on the hull hydrodynamic performances, the width of the initial SR (0.11 m, V6) has been extended to 0.15 m (V4) and 0.19 (V3). In terms of ship resistance, the lower drag has been shown by the V4 for the range speed of 16 to 36 kn, but for the computed higher speed (40 kn), V6 experienced the minimum resistance. One important aspect for this particular case is the propeller shaft inclination of 13°. Moreover, the boat dynamic trim contributes to the increase in the shaft angle, which, by superposing effects, can reach very high inclinations with a negative influence on propeller efficiency. So, the decrease in the trim angle by 0.5° experienced by V4 should be seen as a benefit in terms of propulsion efficiency.
3. In order to study the effects of the whisker rails on the hull hydrodynamic performances, the boat has been equipped with one pair of whisker rails. Total resistance improvement of the hull with WR was by about 2% for the speed range of 20 to 40 kn.
4. To further investigate the effects of the WR on the hydrodynamic performances of the planing boat, two pairs of WR have been mounted on the bare hull of V4. Based on the findings from the study of one pair of WR, the shapes of the WR have been improved leading and trailing edge. In this case, mainly due to the friction reduction, a total resistance reduction of 2.5% to 9.7 % has been reached for the speed range of 32–40 kn.
5. Another approach to reduce the ship resistance of a planing boat is to modify the longitudinal position of the center of gravity. The change of the LOG by 0.2 m aft, led to a ship resistance reduction of 0.5–3.7% for the speed range of 24–40 kn. One important aspect that should be considered, in this particular case, is that the trim angle significantly increases at lower speeds (12–20 kn).
6. Based on the studies presented in the report and the design restriction, the hull version V7, which benefits from the performances of V4 and the improvement brought by the two pairs of whisker rails, can be considered the most effective from the hydrodynamic point of view due to a maximum drag reduction of 9.7% at 40 kn and of 5.9% at 36 kn. On top of that, the drag can still be reduced by moving the center of gravity toward the stern, but the price of increasing the trim should be played off.

Author Contributions: Conceptualization, F.P.; methodology, F.P., A.M. and A.B.; software, F.P., A.M. and A.B.; validation, F.P. and A.B.; formal analysis, F.P. and A.B.; investigation, F.P., A.M. and A.B.; resources, F.P.; data curation, F.P. and A.M.; writing—original draft preparation, F.P., A.M. and A.B.; writing—review and editing, F.P., A.M. and A.B.; visualization, F.P., A.M. and A.B.; supervision, F.P.; project administration, F.P. All authors have read and agreed to the published version of the manuscript.

Funding: This research received no external funding.

Acknowledgments: This research study was performed under the framework of the Naval Architecture Research Center (CCAN) of the Faculty of Naval Architecture, "Dunarea de Jos" University of Galati, Romania. https://www.unicer.ugal.ro/index.php/ro/prezentare-ccan (accessed on 30 September 2022).

Conflicts of Interest: The authors declare no conflict of interest.

References

1. Sottorf, W. *Experiments with Planing Surfaces*; Report No. NACA-TM-661; NASA: Washington, DC, USA, 1934; Report No. NACA-TM-661.
2. Shoemaker, J. *Tank Tests of Flat and V-Bottom Planing Surfaces*; Report No. NACA-TN-509; NASA: Washington, DC, USA, 1934.
3. Sambraus, A. *Planing-Surface Tests at Large Froude Numbers-Airfoil Comparison*; Report No. NACA-TM-848; NASA: Washington, DC, USA, 1938.

4. Savitsky, D.; Brown, P.B. Procedure for Hydrodynamic Evaluation of Planing Hulls in Smooth and Rough Water. *Mar. Technol.* **1976**, *13*, 381–400. [CrossRef]
5. Savitsky, D.; De Lorme, M.F.; Datla, R. Inclusion of Whisker Spray Drag in Performance Prediction Method for High-Speed Planing Hulls. *Mar. Technol. SNAME* **2007**, *44*, 35–56. [CrossRef]
6. Savitsky, D.; Morabito, M. Origin and Characteristics of the Spray Patterns Generated of Planing Hulls. *SNAME Trans. J. Ship Prod. Des.* **2012**, *27*, 63–83. [CrossRef]
7. Savitsky, D. Hydrodynamic Design of Planing Hulls. *Mar. Tech.* **1964**, *1*, 71–94. [CrossRef]
8. Clement, E.P.; Blount, D.L. Resistance Tests of Systematic Series of Planing Hull Forms. *Trans. SNAME* **1963**, *71*, 491–579.
9. Hadler, J.B.; Hubble, E.N.; Holling, H.D. *Resistance Characteristics of A Systematic Series of Planing Hull Forms-Series 65*; SNAME Paper No. 259; Naval Ship Research and development Center: Bethesda, MD, USA, 1974.
10. Keuning, J.A.; Gerritsma, J.; van Tervisga, P.F. *Resistance Tests of a Series Planing Hull Forms with 30 degrees Deadrise Angle, and A Calculation Model Based on this and Similar Systematic Series*; MEMT 25, Report No. 959; Faculty of Marine Technology, Ship Hydromechanics Laboratory: Delft, The Netherlands, 1993.
11. Metcalf, B.J.; Faul, L.; Bumiller, E.; Slutsky, J. *Resistance Tests of a Systematic Series of U.S. Coast Guard Planing Hulls*; Report No. NSWCCD-50-TR-2005/063; Carderock Division, Naval Surface Warefare Center: Potomac, MD, USA, 2005.
12. Taunton, D.J.; Hudson, D.A.; Shenoi, R.A. Characteristics of a series of high speed hard chine planing hulls—Part 1: Performance in calm water. *Int. J. Small Craft Technol* **2010**, *152*, 55–75.
13. De Luca, F.; Pensa, C. The Naples warped hard chine hulls systematic series. *Ocean Eng.* **2017**, *139*, 205–236. [CrossRef]
14. Yousefi, R.; Shafaghat, R.; Shakeri, M. Hydrodynamic analysis techniques for high-speed planing hulls. *Appl. Ocean. Res.* **2013**, *42*, 105–113. [CrossRef]
15. Tulin, M.P. *The Theory of Slender Surfaces Planing at High Speeds*; Department of the Navy: Washington DC, USA, 1957; pp. 125–133.
16. Mauro, H. *High and Low Aspect Ratio Approximation of Planing Surface*; Schiffstechnik: Delft, The Netheland, 1967; pp. 57–64.
17. Wang, D.P.; Rispin, P. Three-Dimensional Planing At High Froude Number. *J. Ship Res.* **1971**, *15*, 221–230. [CrossRef]
18. Cheng, X.; Wellicome, J.F. Study of Planing Hydrodynamics using Strips of Transversely Variable Pressure. *J. Ship Res.* **1994**, *38*, 30–41. [CrossRef]
19. Doctors, L.J. Representation of three-dimensional planing surface by finite elements. In Proceedings of the 1st International Conference on Numerical Ship Hydrodynamics, Gaithersburg, MD, USA, 20–22 October 1975.
20. Xie, N.; Vassalos, D.; Jasionowski, A. A study of Hydrodynamics of Three-Dimensional Planing Surface. *Ocean Eng.* **2005**, *32*, 1539–1555. [CrossRef]
21. Zhao, R.; Faltinsen, O.M.; Haslum, H.A. A Simplified Nonlinear Analysis of a High- Speed Planing Hull in Calm Water. In Proceedings of the 4th International Conference on Fast Sea Transportation (FAST'97), Sydney, Australia, 21–23 July 1977.
22. Ghassemi, H.; Ghiasi, M. A combined method for the hydrodynamic characteristics of planing crafts. *Ocean Eng.* **2008**, *35*, 310–322. [CrossRef]
23. Ghassemi, H.; Su, Y.-M. Determining the Hydrodynamic Forces on a Planing Hull in Steady Motion. *J. Mar. Sci. Appl.* **2008**, *7*, 147–156.
24. Ghassemi, H.; Kohansal, A.R.; Ghamari, I. Nonlinear free surface flows due to the lifting and non-lifting moving bodies. In Proceedings of the 17th Annual International Conference on Mechanical Engineering—ISME2009, Tehran, Iran, 7 May 2009.
25. Ghassemi, H.; Kohansal, A.R. Hydrodynamic Analysis of Non-Planing and Planing Hulls by BEM. *Trans. B Mec. Eng.* **2010**, *17*, 41–52.
26. Brizzolara, S.; Villa, D. CFD Simulation of Planing Hulls. In Proceedings of the 7th International Conference On High-Performance Marine Vehicles, Melbourne, FL, USA 13–15 October 2010.
27. Tagliafierro, B.; Mancini, S.; Ropero-Giralda, P.; Domínguez, J.M.; Crespo, A.J.C.; Viccione, G. Performance Assessment of a Planing Hull Using the Smoothed Particle Hydrodynamics Method. *J. Mar. Sci. Eng.* **2021**, *9*, 244. [CrossRef]
28. Caponneto, M. Practical CFD Simulations for planing Hulls. In Proceedings of the 2nd International Euro Conference on High Performance Marine Vehicles, HIPER 2001, Hamburg, Germany, 2–5 May 2021.
29. Azcueta, R. Steady and Unsteady RANSE Simulations for Planing Crafts. In Proceedings of the International Conference on Fast Sea Transportation FAST 2003, Ischia, Italy, 7–10 October 2003.
30. Mancini, S.; De Luca, F.; Rmolini, A. Towards CFD guidelines for planing hull simulations based on the Naples Systematic Series. In Proceedings of the VII International Conference on Computational Methods in Marine Engineering (MARINE 2017), Nantes, France, 15–17 May 2017; pp. 1071–1085.
31. Mancini, S. The Problem of the Verification and Validation Processes of CFD Simulations of Planing Hulls. Ph.D. Thesis, University of Naples Federico II, Department of Industrial Engineering, Napoli, Italy, 2015.
32. Wheeler, M.P.; Matveev, K.I.; Xing, T. Numerical Study of Hydrodynamics of Heavily Loaded Hard-Chine Hulls in Calm Water. *J. Mar. Sci. Eng.* **2021**, *9*, 184. [CrossRef]
33. Cucinotta, F.; Mancini, D.; Sfravara, F.; Tamburrino, F. The Effect of Longitudinal Rails on an Air Cavity Stepped Planing Hull. *J. Mar. Sci. Eng.* **2021**, *9*, 470. [CrossRef]
34. Du, L.; Lin, Z.; Jiang, Y.; Li, P.; Dong, Y. Numerical Investigation on the Scale Effect of a Stepped Planing Hull. *J. Mar. Sci. Eng.* **2019**, *7*, 392. [CrossRef]

35. Yang, D.; Sun, Z.; Jiang, Y.; Gao, Z. A Study on the Air Cavity under a Stepped Planing Hull. *J. Mar. Sci. Eng.* **2019**, *7*, 468. [CrossRef]
36. Wang, J.; Zhuang, J.; Su, Y.; Bi, X. Inhibition and Hydrodynamic Analysis of Twin Side-Hulls on the Porpoising Instability of Planing Boats. *J. Mar. Sci. Eng.* **2021**, *9*, 50. [CrossRef]
37. Fu, T.; Brucker, K.; Mousaviraad, M.; Ikeda-Gilbert, C.; Lee, E.; O'Shea, T.; Wang, Z.; Stern, F.; Judge, C. An Assessment of Computational Fluid Dynamics Predictions of the Hydrodynamics of High-Speed Planing Craft in Calm Water and Waves. In Proceedings of the 30th Symposium on Naval Hydrodynamics Hobart, Tasmania, Hobart, Australia, 2–7 November 2014.
38. Mousaviraad, S.M.; Wang, Z.; Stern, F. URANS Studies of Hydrodynamic Performance and Slamming Loads on High-Speed Planing Hulls in Calm Water and Waves for Deep And Shallow Conditions. *J. Appl. Ocean. Res.* **2015**, *51*, 222–240. [CrossRef]
39. Hosseini, A.; Tavakoli, S.; Dashtimanesh, A.; Sahoo, P.K.; Kõrgesaar, M. Performance Prediction of a Hard-Chine Planing Hull by Employing Different CFD Models. *J. Mar. Sci. Eng.* **2021**, *9*, 481. [CrossRef]
40. Queutey, P.; Visnonneau, M. An interface capturing method for free-surface hydrodynamic flows. *Comput. Fluids* **2007**, *36*, 1481–1510. [CrossRef]
41. Menter, F.R. Zonal two equation kappa-omega turbulence models for aerodynamic flows. In Proceedings of the 24th AIAA Fluid Dynamics Conference, Orlando, FL, USA, 6–9 July 1993.
42. Guilmineau, E.; Deng, G.B.; Leroyer, A.; Queutey, P.; Visonneau, M.; Wackers, J. Influence of the turbulence closures for the wake prediction of a marine propeller. In Proceedings of the 4th International Symposium on Marine Propellers (SMP'15), Austin, TX, USA, 31 May–4 June 2015.
43. ITTC. *Recommended Procedures and Guidelines: Practical Guidelines for Ship CFD Applications*; 7.5-03 02-03, 2011, Rev. 01; ITTC: Rio de Janeiro, Brazil, 2011; pp. 1–18.
44. ITTC. *Recommended Procedures and Guidelines, Uncertainty Analysis in CFD Verification and Validation Methodology and Procedures*; Rev. 03; ITTC: Wuxi, China, 2017; pp. 1–12.
45. Stern, F.; Wilson, R.V.; Coleman, H.W.; Paterson, E.G. Comprehensive approach to verification and validation of CFD simulations—Part 1: Methodology and procedures. *Fluids Eng.* **2001**, *123*, 793–802. [CrossRef]
46. Mossman, E.A.; Randall, L.M. *An Experimental Investigation of the Design Variables for NACA Submerged Duct Entrances*; NACA RM A7I30; NASA: Washington, DC, USA, 1948; pp. 1–64.
47. Blount, D.L. Design of Propeller Tunnels of High-Speed Craft. In Proceedings of the 4th International Conference on Fast Sea Transportation (FAST'97), Sydney, Australia, 21–23 July 1977.